STK4 regulates TLR pathways and protects against chronic inflammation–related hepatocellular carcinoma

Weiyun Li,[1] Jun Xiao,[1] Xin Zhou,[1] Ming Xu,[2] Chaobo Hu,[1] Xiaoyan Xu,[1] Yao Lu,[1] Chang Liu,[1] Shengjie Xue,[1] Lei Nie,[3] Haibin Zhang,[4] Zhiqi Li,[5] Yanbo Zhang,[1] Fu Ji,[2] Lijian Hui,[1] Wufan Tao,[6] Bin Wei,[7,8] and Hongyan Wang[1]

[1]Key Laboratory of Systems Biology, Innovation Center for Cell Signaling Network, Institute of Biochemistry and Cell Biology, Shanghai Institutes for Biological Sciences, Chinese Academy of Sciences, Shanghai, China. [2]Renji Hospital, School of Medicine, Shanghai Jiaotong University, Shanghai, China. [3]Hubei Cancer Hospital, Wuhan, Hubei Province, China. [4]Eastern Hepatobilliary Surgery Hospital, Second Military Medical University, Shanghai, China. [5]Huashan Hospital, Fudan University, Shanghai, China. [6]Fudan University, Shanghai, China. [7]Wuhan Institute of Virology, Chinese Academy of Sciences, Wuhan, China. [8]State Key Laboratory of Cell Biology, Institute of Biochemistry and Cell Biology, Shanghai Institutes for Biological Sciences, Chinese Academy of Sciences, Shanghai, China.

Hepatocellular carcinoma (HCC) is frequently associated with pathogen infection–induced chronic inflammation. Large numbers of innate immune cells are present in HCCs and can influence disease outcome. Here, we demonstrated that the tumor suppressor serine/threonine-protein kinase 4 (STK4) differentially regulates TLR3/4/9-mediated inflammatory responses in macrophages and thereby is protective against chronic inflammation–associated HCC. STK4 dampened TLR4/9-induced proinflammatory cytokine secretion but enhanced TLR3/4-triggered IFN-β production via binding to and phosphorylating IL-1 receptor–associated kinase 1 (IRAK1), leading to IRAK1 degradation. Notably, macrophage-specific Stk4 deletion resulted in chronic inflammation, liver fibrosis, and HCC in mice treated with a combination of diethylnitrosamine (DEN) and CCl_4, along with either LPS or *E. coli* infection. STK4 expression was markedly reduced in macrophages isolated from human HCC patients and was inversely associated with the levels of IRAK1, IL-6, and phospho-p65 or phospho-STAT3. Moreover, serum STK4 levels were specifically decreased in HCC patients with high levels of IL-6. In STK4-deficient mice, treatment with an IRAK1/4 inhibitor after DEN administration reduced serum IL-6 levels and liver tumor numbers to levels similar to those observed in the control mice. Together, our results suggest that STK4 has potential as a diagnostic biomarker and therapeutic target for inflammation-induced HCC.

Introduction

The persistent presence and amplification of inflammation can predispose cells to oncogenic transformation and contribute to tumor development. Up to 25% of cancers are linked to the persistent presence or amplification of chronic inflammation, including colorectal cancer, gastric carcinoma and hepatocellular carcinoma (HCC) (1). The transcription factor NF-κB is one of the most critical factors that is involved in the context-dependent modulation of many inflammation-induced cancers. Mutations in or abnormal expression of tumor suppressor genes (TSGs) are common in various types of cancers, and some of them have been suggested to regulate NF-κB–induced inflammation and inflammation-induced tumors. Many TSGs have been identified in HCC, which is one of the well-documented human chronic inflammatory disorder–induced cancers. However, it remains largely unknown which TSGs are critical to preventing chronic inflammation–associated HCC at the early stages (2).

Infection with hepatitis B virus or hepatitis C virus is the leading cause of HCC. Other pathogenic microorganisms, such as intestinal bacteria, have also been suggested to promote HCC progression through TLR4 signaling, leading to increased proliferation and prevention of apoptosis (3). In response to these invading pathogens and during the development of chronic inflammation–associated HCC, innate immune cells — especially macrophages — play a critical role not only mediating the inflammatory response, but also engulfing and eliminating microbes. Recent efforts have revealed multiple negative molecules that suppress harmful and excessive inflammatory insults during TLR-induced innate immune responses (4–6). Among them, several innate immune regulators have been suggested to play dual roles, blocking inflammation-driven tumorigenicity by targeting tumor cells in a cell-intrinsic fashion and targeting macrophages to inhibit procarcinogenic inflammation (7–9).

Because substantial numbers of macrophages are present in the liver tumor, and several key TSGs in HCC have abundant expression in immune cells, we investigated whether TSG expression levels in macrophages are associated with microbe infection. Previous studies have identified that WT p53 strongly attenuates NF-κB activation and inhibits the transcription of proinflammatory cytokines and chemokines (10). In agreement with this, the common mutant p53 isoform is frequently identified in human cancers, and the mutant p53 prolongs NF-κB activation, causes severe chronic inflammation, and promotes the development of

Authorship note: Weiyun Li and Jun Xiao contributed equally to this work.
Conflict of interest: The authors have declared that no conflict of interest exists.
Submitted: January 27, 2015; **Accepted:** August 28, 2015.
Reference information: *J Clin Invest*. 2015;125(11):4239–4254. doi:10.1172/JCI81203.

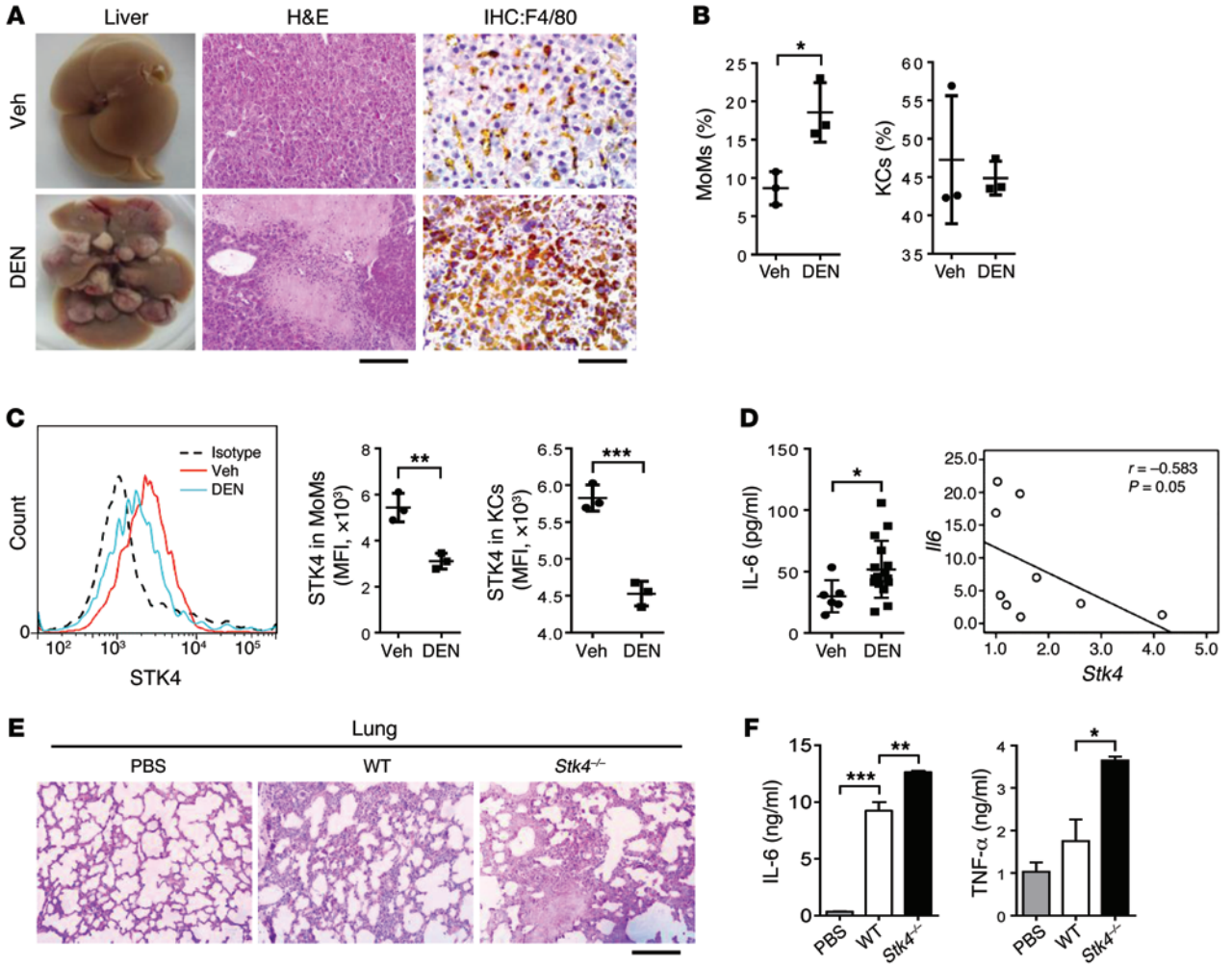

Figure 1. Reduced STK4 expression is associated with DEN-induced HCC and excessive inflammation. (**A**–**C**) WT male mice were treated with controls (Veh) or DEN (50 mg/kg) to induce HCC and were sacrificed 11 months after DEN injection (n = 3). (**A**) HE staining (scale bar: 100 μm) or IHC staining with anti-F4/80 (scale bar: 50 μm) of mouse livers. (**B** and **C**) Percentages of intrahepatic MoMs or KCs, and STK4 expression levels were analyzed by FACS. (**D**) Eleven months after Veh (n > 4) or DEN (n > 7) treatment, serum IL-6 concentrations were detected by ELISA. The correlation of *Il6* and *Stk4* mRNA levels in intrahepatic immune cells were analyzed by Spearman's test (n = 9). (**E** and **F**) Ten hours after LPS challenge (3 mg/mouse, i.p.) of WT (n = 3) and *Stk4*$^{-/-}$ mice (n = 3), HE staining of lungs (scale bar: 100 μm) or serum IL-6 and TNF-α concentrations were measured. Values are mean ± SD from 2 independent experiments. Data represent mean ± SD. *P < 0.05, **P < 0.01, and ***P < 0.001, using 2-tailed, unpaired Student's t test (**B**–**D**) or 1-way ANOVA with Holm-Sidak's multiple comparisons test (**F**).

inflammation-associated colon cancer (11). We found that *Stk4* (serine/threonine-protein kinase 4, also termed mammalian sterile 20–like kinase-1) has a similar expression pattern to *p53* in macrophages (Supplemental Table 1 and Supplemental Figure 1A; supplemental material available online with this article; doi:10.1172/JCI81203DS1). STK4 has been identified to be a tumor suppressor in HCC (12, 13), breast cancer, and lymphoma (14) that regulates cell differentiation and apoptosis. Interestingly, STK4 is also highly expressed in hematopoietic cells to promote naive T lymphocyte proliferation and survival (15, 16) and forms a signaling complex with the RapL/Rap1 module to activate the integrin LFA-1 for lymphocyte adhesion and trafficking (17–22). In this study, we focused on whether and how STK4 in macrophages suppresses inflammation and thereby inhibits chronic inflammation–associated HCC using 2 murine liver tumor models, as well as human HCC patient samples.

Results

Reduced STK4 expression is associated with diethylnitrosamine-induced HCC and excessive inflammation. Viral or bacterial infection–induced HCC is associated with immune cell infiltration and chronic inflammation of the liver. According to the data provided by the Cancer Genome Atlas (TCGA) Research Network program, a series of TSGs have been identified in HCC. We selected 16 TSGs, based on their abundant expression levels in macrophages, to investigate which TSGs play dual roles: blocking inflammation-driven tumorigenicity by targeting both tumor cells and macrophages. Because the tumor suppressor p53 has been revealed to be a key element that regulates both inflammation and tumor growth, we compared *p53* expression levels with 15 other TSGs in mouse primary peritoneal exudate macrophages (PEMs) after *E. coli* infection. Similar to the expression pattern of *p53*, mRNA levels of *Stk4*, *Rap1* (23), *Pten*, *Rhoa*, *Rb*, *Lkb1*, *Trim24*, and *Axin1*

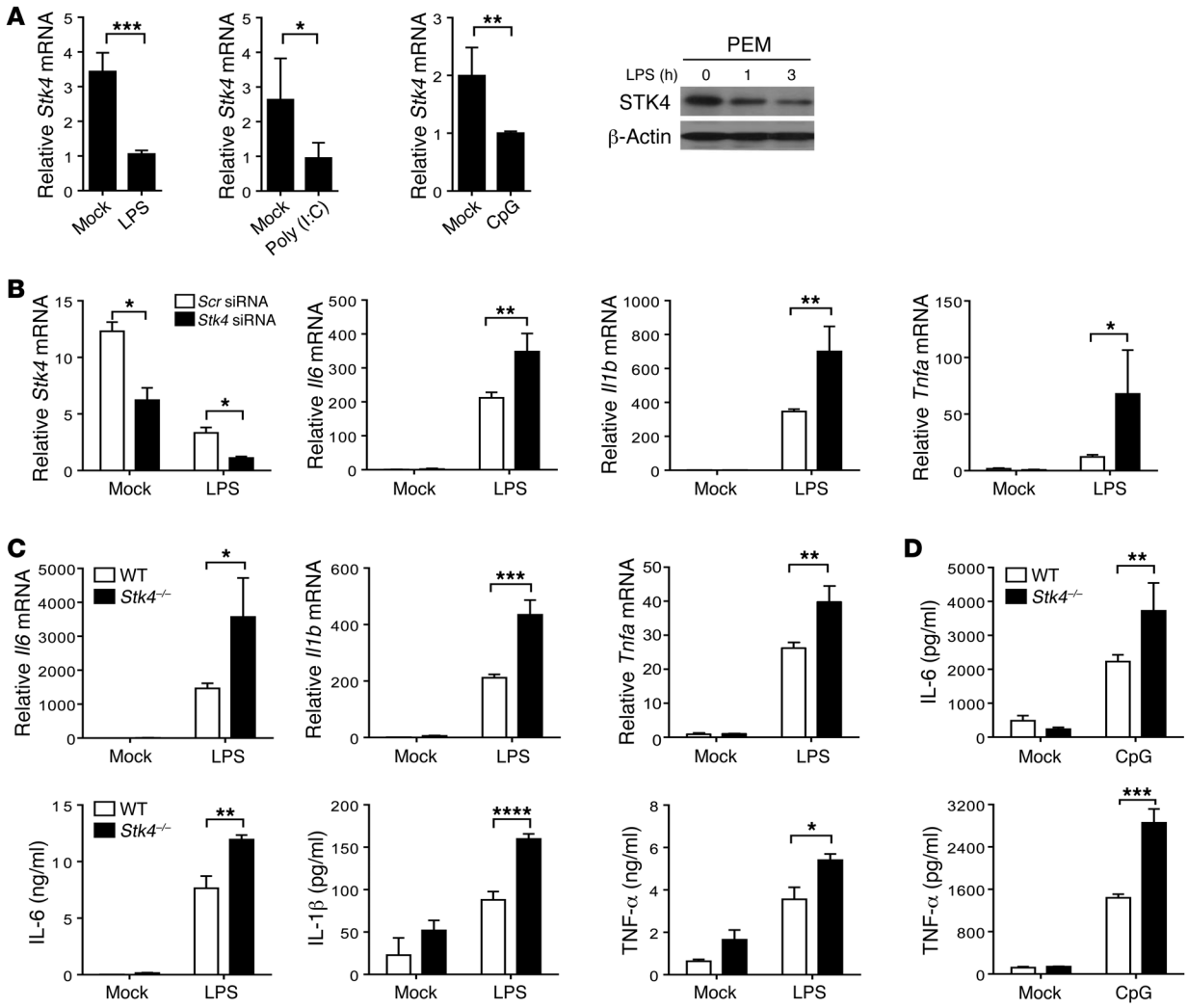

Figure 2. STK4 dampens TLR4/9-induced proinflammatory cytokine production. (**A**) Stk4 expression at mRNA level or protein level was assessed in PEMs, which were stimulated with 1 μg/ml LPS, 10 μg/ml poly(I:C), or 2 μg/ml CpG ODN for 6 hours. (**B**) PEMs were transfected with *Stk4* siRNA or the scramble control (40 nM) followed by LPS stimulation for 6 hours to assess mRNA levels of *Stk4*, *Il6*, *Il1b*, and *Tnfa*. (**C** and **D**) WT and *Stk4*$^{-/-}$ BMMs were stimulated with 1 μg/ml LPS (**C**) or 2 μg/ml CpG ODN (**D**) for 6 hours to detect IL-6, IL-1β, and TNF-α expression by qRT-PCR or ELISA. Data represent mean ± SD ($n \geq 4$). *$P < 0.05$, **$P < 0.01$, ***$P < 0.001$, and ****$P < 0.0001$ using 2-tailed, unpaired Student's *t* test.

were markedly decreased in *E. coli*–infected macrophages (Supplemental Table 1 and Supplemental Figure 1A). The mRNA levels of *Dlc1/2*, *p16*, and *Pax5* were not significantly changed (Supplemental Figure 1B). In contrast, the mRNA levels of *Atip* and *Runx3* were increased compared with those in resting macrophages (Supplemental Figure 1C).

Similar to the suppressive function of p53 in tumor growth and the inflammatory response, previous studies have demonstrated that loss of LKB1 promotes inflammatory cytokine production in T lymphocytes (24) and that AXIN1 also has a preventative effect on inflammation (25). Although STK4 was reported to be a liver tumor suppressor and is expressed in immune cells, it remains unclear whether STK4 inhibits infection-induced inflammation in macrophages and thereby suppresses the pathological process of inflammation-associated HCC.

To answer this question, we used the diethylnitrosamine-induced (DEN-induced) liver cancer model to check macrophage infiltration and the expression level of STK4. Eleven months after DEN injection, the majority of the mice developed liver neoplasias, and HE staining showed severe liver damage with immune cell infiltration (Figure 1A, left panel). By IHC analysis using anti-F4/80^{+} antibody, we confirmed the enhanced accumulation of intrahepatic macrophages during DEN-induced hepatocarcinogenesis compared with vehicle-treated mice (Figure 1A). According to a previous report (26), we further identified by FACS analysis that the percentage of monocyte-derived macrophages (MoMs, defined as F4/80^{+}CD11b^{hi}Ly6c^{int}) was increased, whereas the percentage of liver-resident Kupffer cells (KCs, defined as F4/80^{+}CD11b^{lo}Ly6c^{lo}) was not significantly changed (Figure 1B and Supplemental Figure 1D). Importantly, a significant reduction of STK4 expression was observed in both MoMs and KCs (Figure 1C and Supplemental Figure 1E). The STK4 expression levels were also assessed in other immune cell lineages and were reduced in T cells but not in NK or B cells (Supplemental Figure 1F). More-

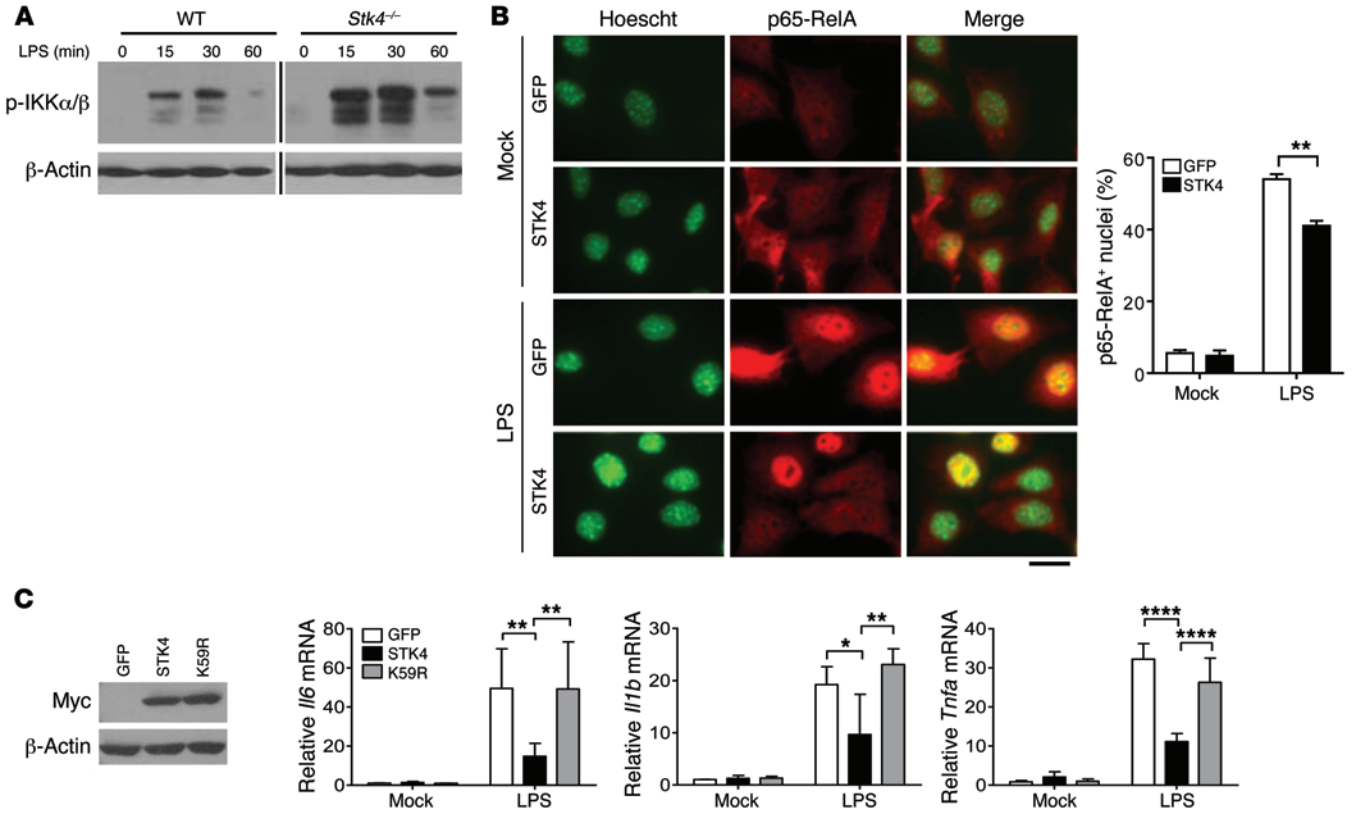

Figure 3. STK4 kinase activity is critical to inhibit TLR4/NF-κB activation. (**A**) The levels of phosphorylated IKKα/β in LPS-stimulated WT and *Stk4*$^{-/-}$ BMMs were detected by immunoblotting analysis. Samples were run on the same gel but not contiguous, as indicated by the black line. (**B**) Primary MEF cells overexpressing GFP or STK4 were treated with or without LPS, followed by immunostaining with Hoechst and anti–p65-RelA (scale bar: 20 μm, representative images). The number of p65-RelA^{+} nuclei was counted from >50 cells (mean ± SD using 2-tailed, unpaired Student's *t* test). (**C**) Primary MEFs overexpressing GFP, STK4, or the K59R mutant were stimulated with LPS to detect mRNA levels of *Il6*, *Il1b*, and *Tnfa*. Values were normalized for β-actin mRNA levels (mean ± SD, *n* = 4, 2-way ANOVA with Holm-Sidak's multiple comparisons test). **P* < 0.05, ***P* < 0.01, and ****P* < 0.0001.

over, in the early stage after DEN treatment — at 5 weeks — STK4 expression was also decreased in MoMs, KCs, and T cells, but not in B cells (Supplemental Figure 1, G and H). Next, we found that serum concentrations of IL-6 in DEN-treated mice were much higher than in the vehicle controls. Moreover, *Il6* mRNA levels inversely correlated with mRNA levels of *Stk4* in intrahepatic immune cells (Figure 1D). This correlation led us to further investigate whether STK4 plays a direct role in downregulating inflammation. WT and *Stk4*-deficient mice were challenged with lipopolysaccharide (LPS), the major component of gram-negative bacteria. *Stk4*-deficient mice displayed more severe lung damage with enhanced infiltration of immune cells in the lungs (Figure 1E), including macrophages (identified as the CD11b^{+}F4/80^{+} cell population by FACS, data not shown). Serum concentrations of IL-6 and TNF-α were also elevated in LPS-treated *Stk4*-deficient mice (Figure 1F). These data together led us to examine whether the tumor suppressor STK4 might inhibit macrophage-mediated inflammation during innate immune responses against infections and protect the host from chronic inflammation–induced HCC.

STK4 kinase activity is critical to dampening TLR4/9-induced proinflammatory cytokine production. Recent studies have shown that TLR4 contributes to bacterial infection–induced inflammation, which drives liver tumor promotion (3). Furthermore, the TLR3/4/9 pathways are associated with HBV (a DNA virus) or HCV (an RNA virus) infection–induced HCC (27). We therefore examined whether the expression and function of STK4 is linked to TLR signaling–triggered inflammation. WT macrophages were treated with LPS, poly(I:C), or CpG, respectively, to mimic infection with bacteria or viruses. We observed a significant decrease in *Stk4* expression at the mRNA level in response to TLR3/4/9 agonists (Figure 2A, left panels). Reduced protein levels of STK4 in LPS-stimulated macrophages were confirmed by immunoblotting (Figure 2A, right panel). Interestingly, after *p65* was knocked down using a specific siRNA, LPS-stimulated macrophages still exhibited decreased mRNA levels of *Stk4* (Supplemental Figure 2A). This suggests that TLR4 signaling regulates STK4 expression independently of p65.

Next, specific siRNA was used to knock down *Stk4* in mouse PEMs, and the knockdown efficiency was confirmed by RT-PCR analysis (Figure 2B). Knockdown of *Stk4* significantly enhanced mRNA levels of *Il6*, *Il1b*, and *Tnfa* in response to LPS stimulation (Figure 2B). In agreement with this, when Myc-tagged STK4 was stably overexpressed in RAW264.7 cells (Supplemental Figure 2B, left panel), mRNA levels of *Il6*, *Il1b*, and *Tnfa* were decreased after LPS stimulation (Supplemental Figure 2B, right panels). To further confirm this phenotype, *Stk4*-deficient macrophages were

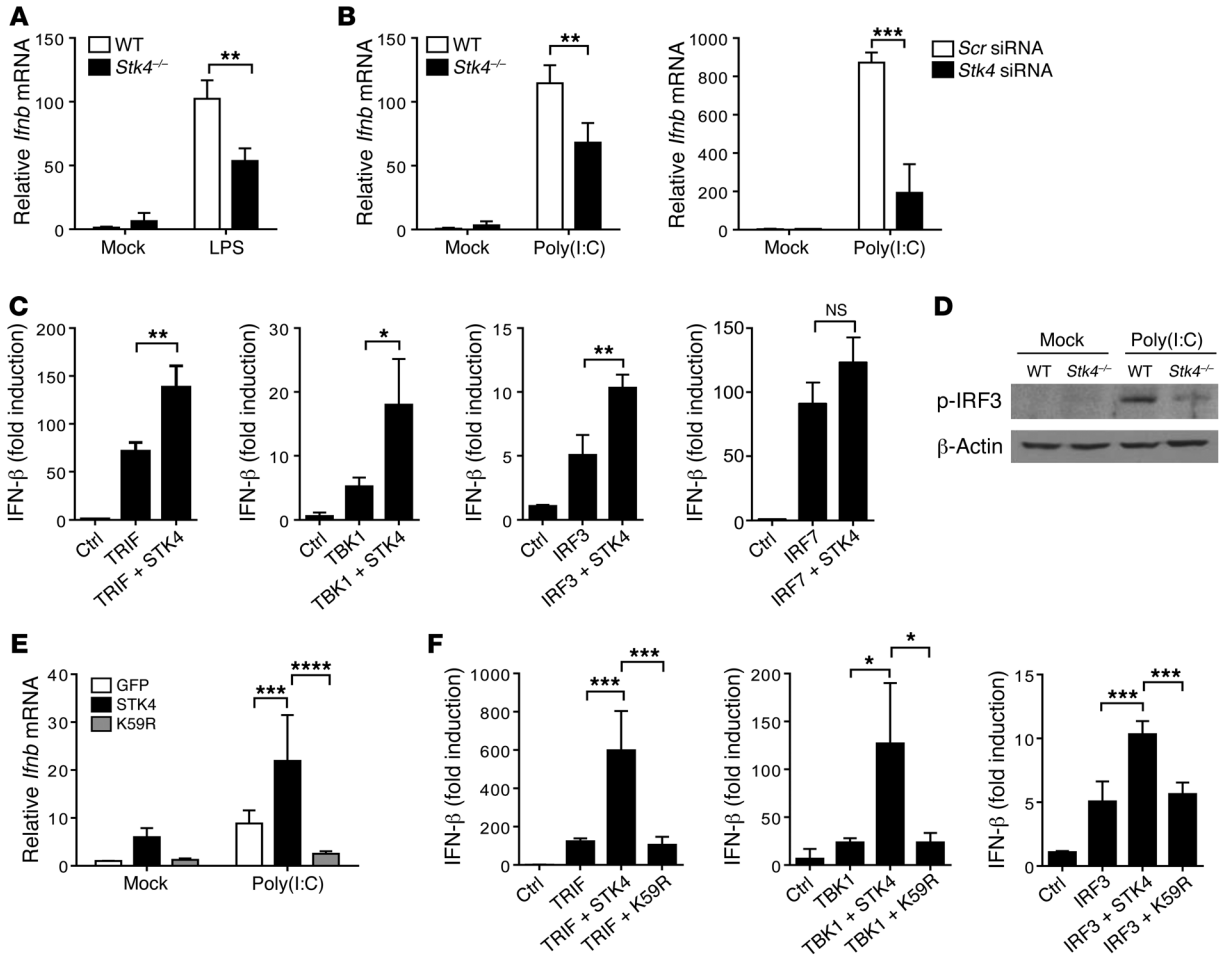

Figure 4. STK4 increases TLR3/4-induced IFN-β production in macrophages. (**A**) WT and *Stk4*$^{-/-}$ BMMs were stimulated with LPS for 3 hours to evaluate mRNA levels of *Ifnb* by qRT-PCR. (**B**) WT and *Stk4*$^{-/-}$ BMMs (left), or PEMs transfected with *Stk4* siRNA or scramble siRNA (right) were exposed to poly(I:C) for 3 hours to assess *Ifnb* mRNA levels. (**C**) TRIF, TBK1, IRF3, or IRF7 were overexpressed with STK4 and the IFN-β luciferase reporter plasmid in HEK293T cells to measure IFN-β luciferase activity. The cotransfected Renilla was used as an internal control. (**D**) IRF-3 phosphorylation levels in poly(I:C)-treated WT or *Stk4*$^{-/-}$ BMMs were checked by immunoblotting analysis. (**E**) Primary MEF cells overexpressing GFP, STK4, or the K59R mutant were stimulated with poly(I:C) to determine *Ifnb* mRNA levels. (**F**) TRIF, TBK1, and IRF3 were transfected with STK4 or K59R and the IFN-β luciferase reporter plasmid into HEK293T cells to measure IFN-β luciferase activity. Data represent mean ± SD ($n \geq 3$). *$P < 0.05$, **$P < 0.01$, ***$P < 0.001$, and ****$P < 0.0001$ using 2-tailed, unpaired Student's *t* test (**A**–**C**), 2-way ANOVA (**E**), or 1-way (**F**) with Holm-Sidak's multiple comparisons test.

prepared and stimulated with LPS. *Stk4* deficiency significantly promoted the production of *Il6*, *Il1b,* and *Tnfa* at the mRNA and protein levels (Figure 2C). Interestingly, *Stk4*-deficient macrophages also augmented IL-6 and TNF-α secretion in response to CpG (i.e., TLR9 agonist) treatment compared with WT cells (Figure 2D). Because our previous study showed that poly(I:C) induces proinflammatory cytokine production at much lower levels (6), we did not focus on STK4-mediated proinflammatory cytokine production via the poly(I:C)/TLR3 pathway.

We then assessed whether *Stk4* deficiency affected TLR4/9-induced production of proinflammatory cytokines via NF-κB activation. LPS-stimulated *Stk4*-deficient macrophages elevated phosphorylation levels of IKKα and IKKβ compared with those in WT controls (Figure 3A). We next overexpressed STK4 or the control GFP in primary mouse embryonic fibroblasts (MEFs) and measured numbers of cells showing significant p65 translocation into the nucleus after LPS stimulation. Nuclear import of p65 was significantly increased in the GFP control MEFs in response to LPS, whereas STK4 overexpression suppressed this enhancement (Figure 3B). In contrast, no significant changes in phosphorylation levels of ERK and JNK were observed between *Stk4*-deficient and WT macrophages (Supplemental Figure 3A). This suggests that STK4 does not affect MAPK activation in LPS-treated macrophages.

Because surface TLR4 expression or TLR4 degradation has been demonstrated to regulate NF-κB activation (28, 29), we next tested whether STK4 could modulate TLR4 expression levels. There were no detectable changes in the total protein or mRNA levels of *Tlr4* between WT and *Stk4*-deficient macrophages (Supplemental Figure 3B). Flow cytometry analysis showed that *Stk4* deficiency slightly increased TLR4 surface expression in unstimulated macrophages. After LPS stimulation, reduction of surface TLR4 levels was markedly dampened in *Stk4*-deficient macrophages compared with WT cells (Supplemental Figure 3C). In agreement with this finding, compared with the GFP control

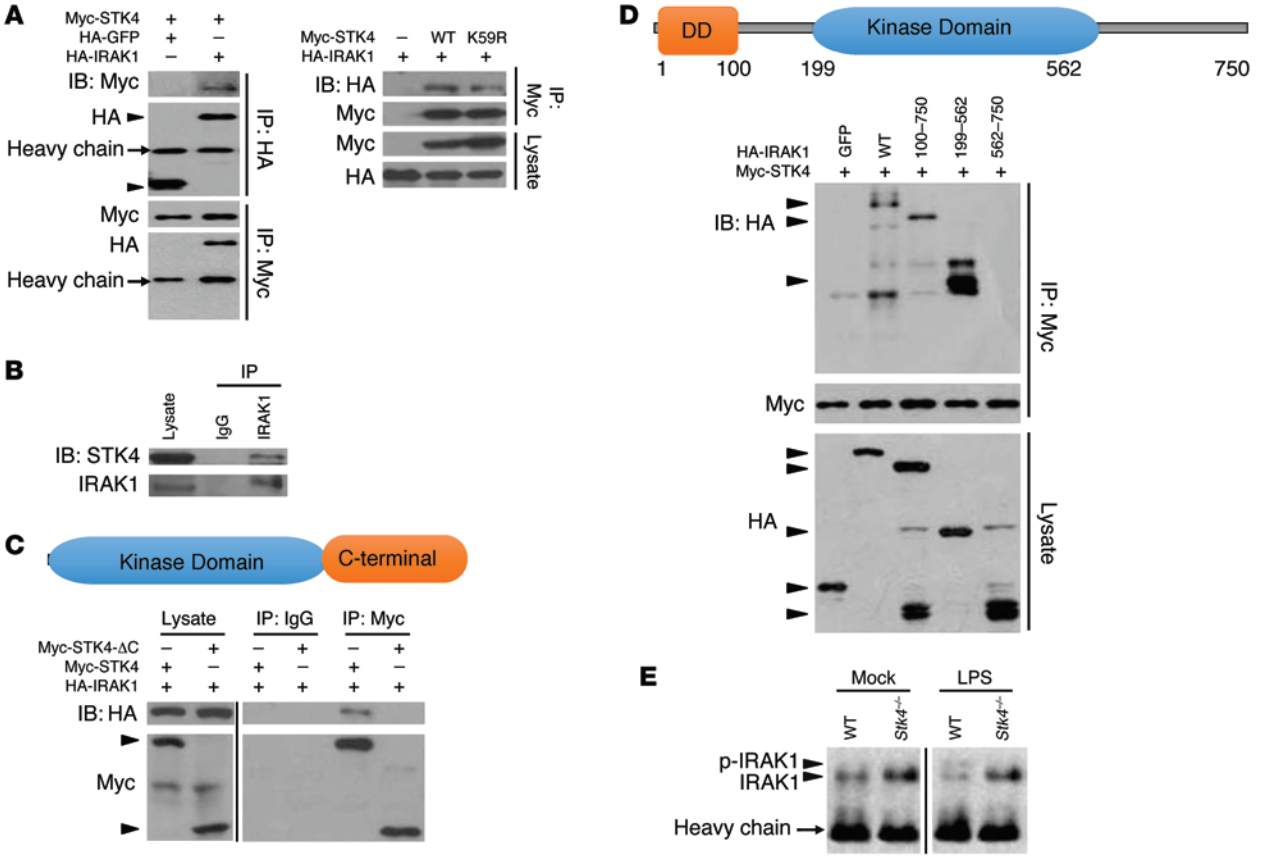

Figure 5. STK4 binds to and phosphorylates IRAK1. (**A**) HEK293T cells overexpressing HA-GFP, HA-IRAK1, Myc-STK4, or Myc-K59R were prepared for immunoprecipitation and immunoblotting with the indicated antibodies. (**B**) Immunoprecipitation was performed using anti-IRAK1 antibody from RAW264.7 cells, followed by immunoblotting with anti-IRAK1 or anti-STK4 antibodies. (**C**) HEK293T cells were transfected with HA-IRAK1 and Myc-STK4 or the C-terminal deletion mutant Myc-STK4-ΔC, followed by immunoprecipitation and immunoblotting with the indicated antibodies. (**D**) HEK293T cells were transfected with Myc-STK4 and HA-IRAK1 or its truncated mutants, including the N-terminal fragment (100-750aa), the kinase domain (199-562aa), and the C-terminal end (562-750aa). Immunoprecipitation using anti-Myc antibody was performed followed by immumoblotting. (**E**) Immunoprecipitation using anti-IRAK1 antibody was performed from WT and *Stk4*$^{-/-}$ BMMs, followed by anti-IRAK1 immunoblotting. Samples were run on the same gel but not contiguous, as indicated by the black line. (**A**–**E**). Data represent the representative experiments from at least 3 independent experiments.

cells, STK4 overexpression decreased TLR4 surface expression in unstimulated or LPS-treated RAW264.7 cells (Supplemental Figure 3D). These results suggest that reduced TLR4 surface expression and NF-κB activation contribute to the suppression of proinflammatory cytokine production by STK4.

Multiple studies have reported that the kinase activity of STK4 is required for cell apoptosis, cell adhesion, and migration via phosphorylation of its downstream targets, including FOXO, AKT, and YAP1 (13, 30, 31). To determine whether STK4 kinase activity is crucial for the production of proinflammatory cytokines, we overexpressed the kinase-dead (KD) mutant of STK4 (termed K59R) and WT STK4 at the same level in primary MEFs (Figure 3C, left panel). Compared with the substantial inhibitory role of WT STK4, the K59R mutant failed to inhibit mRNA levels of *Il6, Il1b,* and *Tnfa* in response to LPS stimulation (Figure 3C, right panels).

STK4 increases TLR3/4-induced IFN-β production in macrophages. It has been revealed that TLR3/4 signaling–induced type-I interferon (IFN) production plays a significant role against HBV or HCV infection. We next assessed whether STK4 regulates the production of IFN-β in LPS or poly(I:C)-stimulated macrophages. Interestingly, in contrast to the inhibitory role of STK4 in the production of proinflammatory cytokines, knockdown of *Stk4*, or deficiency of *Stk4* decreased mRNA levels of *Ifnb* in macrophages in response to LPS or poly(I:C) treatment (Figure 4, A and B). Consistent with this finding, STK4 overexpression enhanced *Ifnb* mRNA levels in LPS-treated RAW264.7 cells (Supplemental Figure 4A). In agreement with our previous report (6), when compared with poly(I:C) treatment, CpG stimulation barely induced *Ifnb* mRNA expression in WT and *Stk4*-deficient macrophages (Supplemental Figure 4B). We therefore propose that STK4 might make a significant contribution to clearance of viral infection via the TLR3/4 signaling pathways and IFN-β production.

Since TRIF, TBK1, IRF3, and IRF7 are key regulators of IFN-β production, we next examined which molecules cooperated with STK4 in the IFN-β luciferase reporter system. TRIF, TBK1, IRF3, or IRF7 were overexpressed with STK4 in HEK293T cells, and the IFN-β luciferase readings were compared with those in cells transfected with the empty vector or plasmids expressing only TRIF, TBK1, IRF3, or IRF7. Interestingly, overexpression of STK4 together with TRIF, TBK1, or IRF3 substantially enhanced IFN-β luciferase readings. In contrast, no significant enhancement was detected when STK4 was coexpressed with IRF-7 (Figure 4C). We then exam-

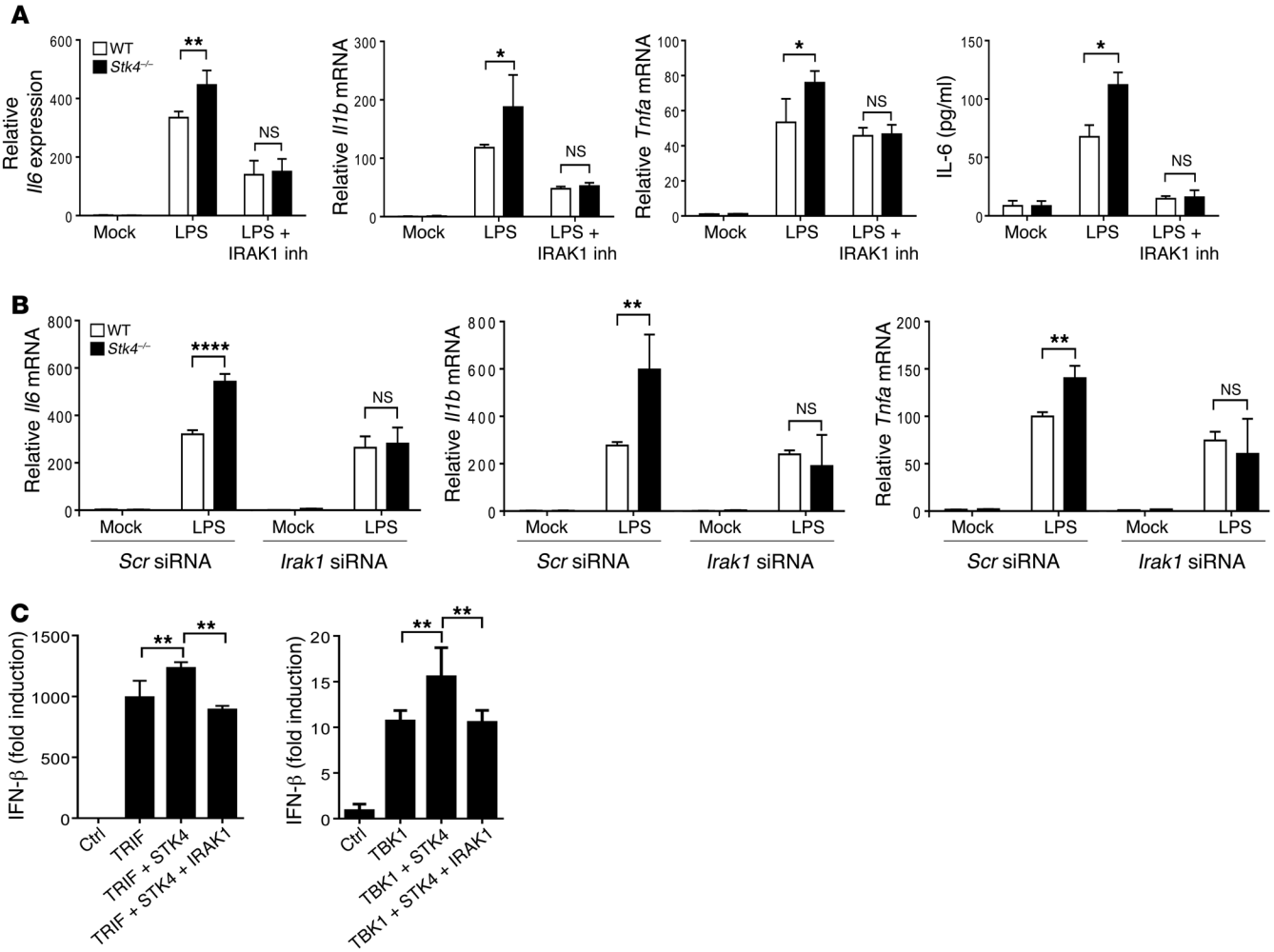

Figure 6. STK4 regulates the TLR3/4 pathways via IRAK1. (**A**) WT and *Stk4*$^{-/-}$ BMMs were preincubated with the IRAK1/4 inhibitor or (**B**) PEMs were transfected with the scramble siRNA or *Irak1* siRNA, followed by LPS treatment for 3 hours to measure mRNA levels of *Il6*, *Il1b*, and *Tnfa* by qRT-PCR or IL-6 concentrations in the supernatants by ELISA. 2-tailed, unpaired Student's *t* test was used. (**C**) STK4, IRAK1, TRIF, and TBK1 were transfected with the IFN-β luciferase reporter into HEK293T cells to measure IFN-β luciferase activity. One-way ANOVA with Holm-Sidak's multiple comparisons test was used. Data represent mean ± SD ($n \geq 4$). *$P < 0.05$, **$P < 0.01$, and ****$P < 0.0001$.

ined whether STK4 regulates the phosphorylation levels of IRF-3 and TBK1. Compared with WT macrophages, *Stk4*-deficient macrophages reduced p-IRF3 levels in response to poly(I:C) stimulation (Figure 4D) and p-TBK1 levels in response to LPS treatment (Supplemental Figure 4C). Next, we determined whether STK4 kinase activity was also needed for IFN-β production. Although WT STK4 enhanced poly(I:C)-induced mRNA levels of *Ifnb*, the K59R mutant significantly blocked this effect (Figure 4E). Moreover, we observed that WT STK4 cooperated with TRIF, TBK1, or IRF3 to further enhance IFN-β luciferase readings, whereas the K59R mutant failed to achieve this effect (Figure 4F). STK3 is the homologue of STK4, which exerted no significant influence on TLR4/9-induced proinflammatory cytokine production or TLR3/4-induced IFN-β production (Supplemental Figure 4D). Taking these findings together, we have demonstrated that STK4 is dependent on TRIF, TBK1, and IRF3 to enhance TLR3/4-mediated production of IFN-β.

STK4 binds to and phosphorylates IRAK1. It was previously reported that IRAK1 (IL-1 receptor–associated kinase 1) is phosphorylated at the serine/threonine (ser/thr) site for degradation, which then results in IRF3 activation and increased IFN-β production (32–35). In contrast to its negative role in IFN-β production, IRAK1 promotes the TLR4-triggered production of proinflammatory cytokines (34–36). We next asked whether the ser/thr kinase STK4 might interact with IRAK1 and thereby promote its phosphorylation and degradation, resulting in differential regulation of the TLR3/4 pathways. Myc-tagged STK4 and HA-tagged IRAK1 were overexpressed in HEK293T cells. Immunoprecipitation using anti-HA (IRAK1) antibodies pulled down Myc-tagged STK4, and vice versa (Figure 5A, left panel). Interestingly, the K59R mutant also pulled down HA-tagged IRAK1 (Figure 5A, right panel). We then confirmed that STK4 interacts with IRAK1 endogenously in RAW264.7 cells (Figure 5B). To map their interaction domains, the C-terminal domain of STK4 was deleted and termed STK4-ΔC, which failed to interact with IRAK1 (Figure 5C). We then truncated IRAK1 into 3 fragments that contained 100–750, 199–562, or 562–750 amino acids of IRAK1 and were tagged with HA. The IRAK1 fragments 100–750 and 199–562 interacted with STK4 but not the fragment 562–750 (Figure 5D).

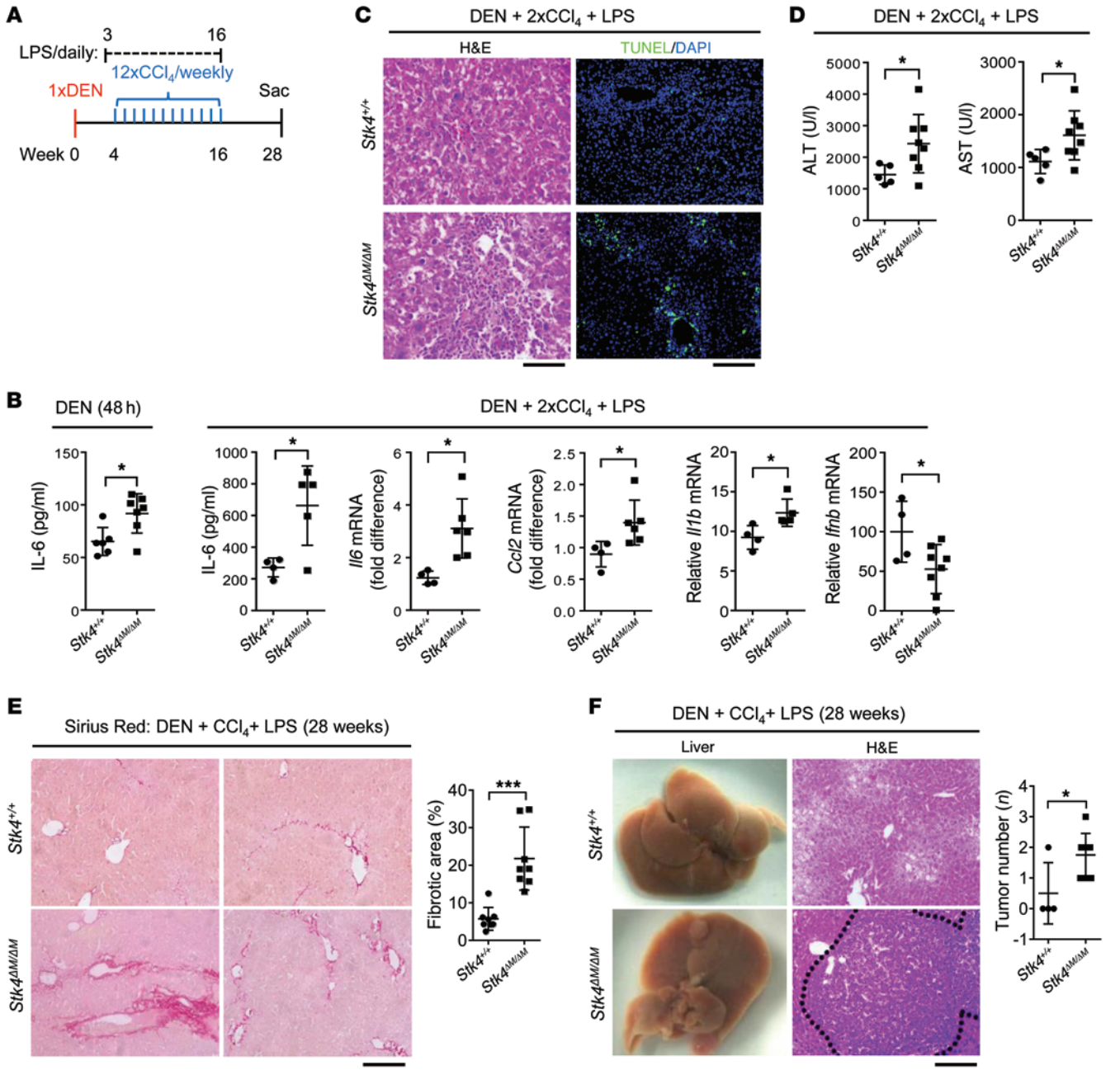

Figure 7. STK4 protects mice from DEN- and LPS-induced HCC in vivo. (**A**) Scheme of the DEN-, CCl_4-, and LPS-induced HCC model. Mice carrying macrophage-specific *Stk4* deletion ($Stk4^{\Delta M/\Delta M}$) and their littermate control ($Stk4^{+/+}$) were i.p. injected with DEN (100 mg/kg). Four weeks later, these mice received weekly i.p. injections of CCl_4 (0.5 ml/kg), plus daily subcutaneous injection of LPS (300 μg/kg, starting 1 week before the first CCl_4 injection) for 12 weeks. Mice were sacrificed 28 weeks after DEN treatment. (**B**) $Stk4^{+/+}$ ($n \geq 4$) and $Stk4^{\Delta M/\Delta M}$ ($n > 5$) mice were treated with DEN for 48 hours, plus 2 weekly injections of CCl_4 and daily injection of LPS. Serum IL-6 levels and mRNA levels of *Il6*, *Il1b*, *Ccl2*, and *Ifnb* in livers were determined. (**C** and **D**) $Stk4^{+/+}$ ($n = 5$) and $Stk4^{\Delta M/\Delta M}$ ($n = 8$) mice were treated with DEN, plus 2 weekly injections of CCl_4 and daily injection of LPS. HE staining (scale bars: 50 μm) and TUNEL assays (scale bar: 100 μm) of liver sections (**C**) or serum ALT and AST levels (**D**) were assessed. (**E** and **F**) $Stk4^{+/+}$ ($n = 4$) and $Stk4^{\Delta M/\Delta M}$ mice ($n = 8$) were treated as described in (**A**) and sacrificed 28 weeks after DEN treatment. Sirius Red staining (**E**) or HE staining (**F**) of liver sections were performed (scale bars: 100 μm). Data represent mean ± SD. $^*P < 0.05$ and $^{***}P < 0.001$ using 2-tailed, unpaired Student's *t* test.

Next, we asked whether phosphorylation and degradation of IRAK1 was impaired in *Stk4*-deficient macrophages. Endogenous IRAK1 was immunoprecipitated from WT and $Stk4^{-/-}$ BM-derived macrophages (BMMs) that were untreated or stimulated with LPS for 40 minutes. IRAK1 was phosphorylated, and its position had shifted, as determined by immunoblotting, after LPS stimulation of WT BMMs. Interestingly, the expression level of IRAK1 decreased in LPS-stimulated WT BMMs, suggesting IRAK1 degradation. In contrast, IRAK1 phosphorylation and degradation was not observed in *Stk4*-deficient BMMs (Figure 5E). Furthermore, overexpression of the K59R mutant failed to induce phosphorylation of IRAK1 compared with overexpression of STK4 (Sup-

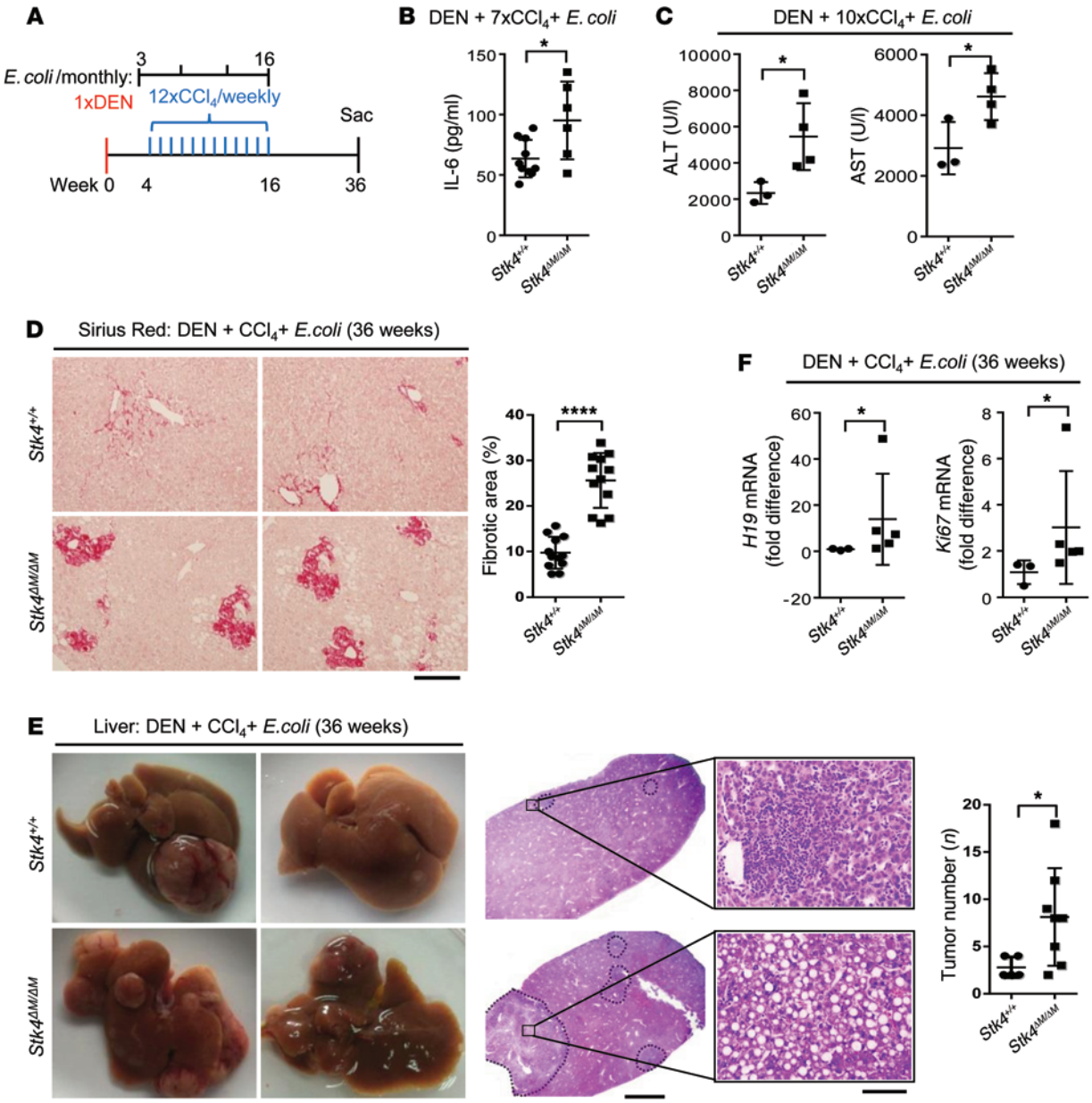

Figure 8. STK4 protects mice from DEN and bacterial infection–induced HCC in vivo. (**A**) Scheme of the DEN, CCl_4, and *E. coli*–induced HCC model. $Stk4^{+/+}$ and $Stk4^{\Delta M/\Delta M}$ mice were injected with DEN (100 mg/kg, i.p.). Four weeks later, these mice received 12 weekly injections of CCl_4 (0.5 ml/kg, i.p.), plus 4 monthly *E. coli* infection (5,000 CFU i.v., starting 1 week before the first CCl_4 injection). Mice were sacrificed 36 weeks after DEN treatment. (**B**) Serum IL-6 concentrations were determined from $Stk4^{+/+}$ (n = 10) and $Stk4^{\Delta M/\Delta M}$ (n = 6) mice, which were treated with DEN, plus 7 injections of CCl_4 and monthly *E. coli* infection. (**C**) $Stk4^{+/+}$ (n = 3) and $Stk4^{\Delta M/\Delta M}$ (n = 4) male mice were treated with DEN, plus 10 injections of CCl_4 and monthly *E. coli* infection. Serum ALT and AST levels were measured to assess liver injury. (**D**–**F**) $Stk4^{+/+}$ ($n \geq 3$) and $Stk4^{\Delta M/\Delta M}$ ($n > 5$) mice were treated with DEN, plus 12 injections of CCl_4 and monthly *E. coli* infection, and sacrificed at 36 weeks. Sirius Red staining (**D**, scale bar: 100 μm) or HE staining (**E**, scale bars: 2 mm [left], 50 μm [right]) of liver sections were shown. qRT-PCR was performed to assess mRNA levels of *H19* and *Ki67* in livers (**F**) ($n \geq 3$). Data represent mean ± SD. $^*P < 0.05$ and $^{****}P < 0.0001$ using 2-tailed, unpaired Student's t test.

plemental Figure 5). These results suggest that the C-terminal domain of STK4 binds to the kinase domain of IRAK1, leading to IRAK1 phosphorylation and degradation.

STK4 regulates the TLR3/4 pathways via IRAK1. We next investigated whether IRAK1 cooperates with STK4 to differentially regulate production of proinflammatory cytokines and IFN-β. WT and *Stk4*-deficient BMMs were pretreated with the IRAK1/4 inhibitor or a DMSO control for 1 hour, then stimulated with LPS for an additional 6 hours. Compared with the DMSO control, the IRAK1/4 inhibitor significantly inhibited mRNA levels of *Il6*, *Il1b*, and *Tnfa*, as well as IL-6 secretion in LPS-induced macrophages. Importantly, the enhancement of IL-6, IL-1β, and TNF-α levels as a result of *Stk4* deficiency was substantially blocked by the IRAK1/4 inhibitor, resulting in similar levels to those found in WT cells (Figure 6A). To further confirm the effect of IRAK1, we silenced *Irak1* expression in WT and $Stk4^{-/-}$ PEMs using specific siRNA (Supplemental Figure

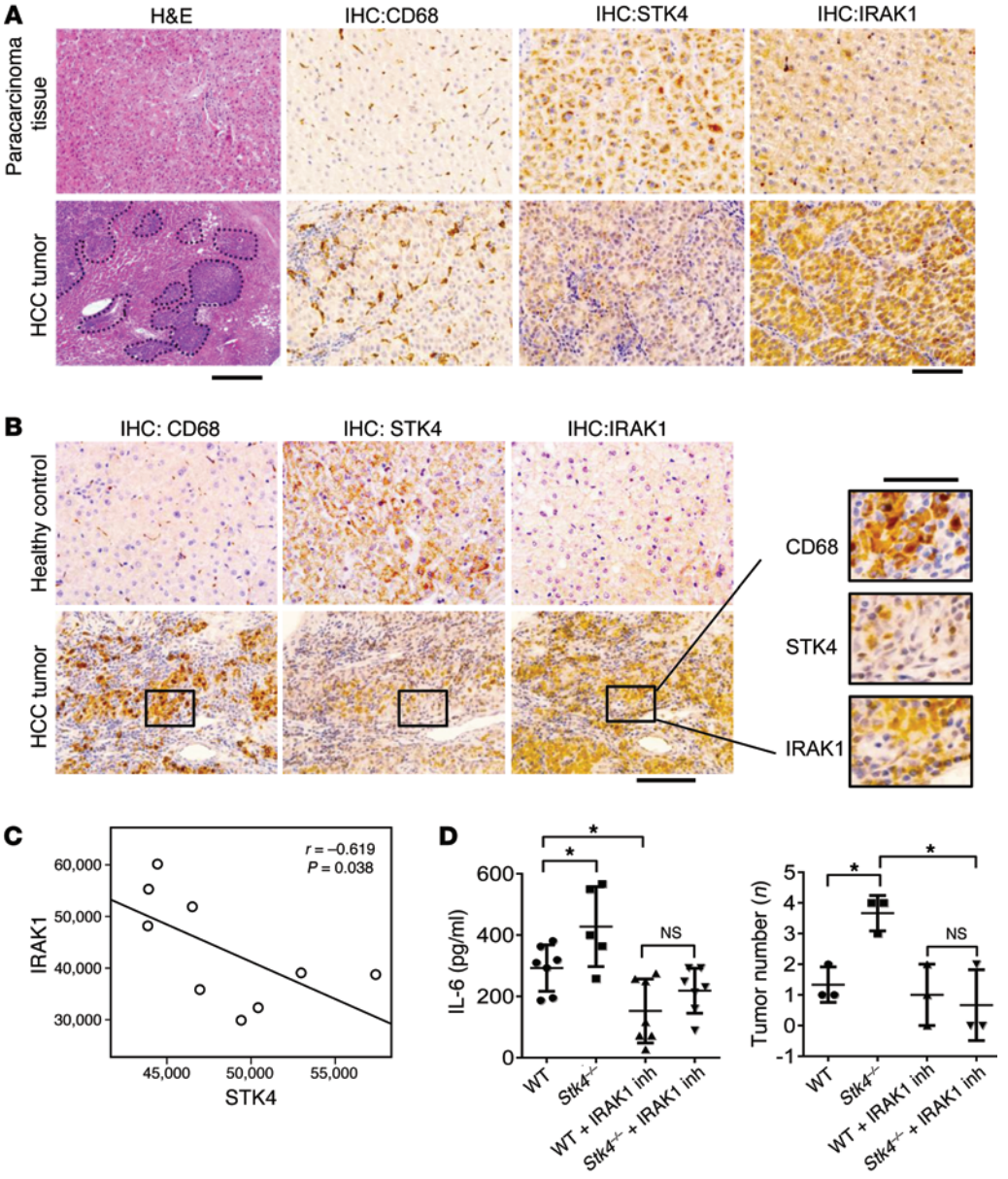

Figure 9. The inverse correlation of STK4 expression with IRAK1 levels in macrophages from human HCC samples. (**A**) HE staining (scale bar: 100 μm) and IHC staining (scale bar: 50 μm) with anti-CD68, anti-STK4, and anti-IRAK1 of human liver sections from paracarcinoma tissue and tumors of HCC patients. (**B**) The adjacent sections from human HCC tumors or healthy livers were stained with anti-CD68, anti-STK4, or anti-IRAK1 (scale bars: 50 μm). (**C**) IRAK1 and STK4 expression in liver-infiltrated macrophages from HCC patients was examined by FACS (n = 9), and their correlation was assessed with Pearson's test. (**D**) Mice were i.p. injected the IRAK1/4 inhibitor (3 mg/kg, twice a week), starting 1 week before the first CCl_4 injection. Serum IL-6 levels (WT [n = 7], *Stk4*$^{-/-}$ [n = 5], WT+IRAK1 Inh [n = 7], and *Stk4*$^{-/-}$ +IRAK1 Inh [n = 7]) were checked 6 weeks after DEN treatment (left panel), and liver tumor formation (n = 3) was detected by micro-CT imaging 18 weeks after DEN treatment (right panel). One-way ANOVA with Newman-Keuls or Holm-Sidak's multiple comparisons test was used. Data represent mean ± SD. *P < 0.05.

6A). After knocking down IRAK1, mRNA levels of proinflammatory cytokines were significantly reduced in *Stk4*-deficient PEMs and were no longer higher than the levels in the control cells (Figure 6B). Consistent with this finding, the concentrations of IL-6 and TNF-α in *Stk4*-deficient PEMs were also substantially dampened by *Irak1* siRNA (Supplemental Figure 6B). Because STK4-ΔC failed to interact with IRAK1 (Figure 5C), we also confirmed that overexpressed STK4-ΔC lost the ability to inhibit mRNA levels of *Il6*, *Il1b*, and *Tnfa* in LPS-treated RAW264.7 cells (Supplemental Figure 6C).

Next, we used the luciferase reporter assay to examine whether IRAK1 cooperates with STK4 for TRIF- or TBK1-induced IFN-β expression. In agreement with previous reports (32, 33), overexpression of IRAK1 with TRIF or TBK1 reduced the IFN-β luciferase readings (Supplemental Figure 6D). We observed that STK4 overexpression indeed enhanced the IFN-β luciferase readings; importantly, overexpression of IRAK1 rescued this effect, resulting in similar levels to those found in samples with TRIF or TBKI alone (Figure 6C). Taken together, our data indicate that STK4 is dependent on its substrate IRAK1 to inhibit proinflammatory cytokine production and increase IFN-β expression.

STK4 protects mice from chronic inflammation–induced HCC in vivo. Accumulated studies have provided convincing evidence elucidating that chronic inflammation plays a critical role in inducing HCC — e.g., liver macrophage–derived IL-6 contributes to HCC development (37–39) — and TNF-α is injurious for induction of hepatocyte apoptosis (40). In addition, IFN-β is suggested to facilitate host clearance of pathogens, including HBV and HCV (41). Because we observed that STK4 impaired IL-6 and TNF-α production (Figures 2 and 3) but enhanced IFN-β levels (Figure 4), it was key to address whether the regulatory role of STK4 in the macrophage-mediated inflammatory response could prevent pathogen infection–associated HCC.

Although loss of STK4 initiates hepatocyte proliferation with dramatic resistance to proapoptotic stimuli, resulting in the devel-

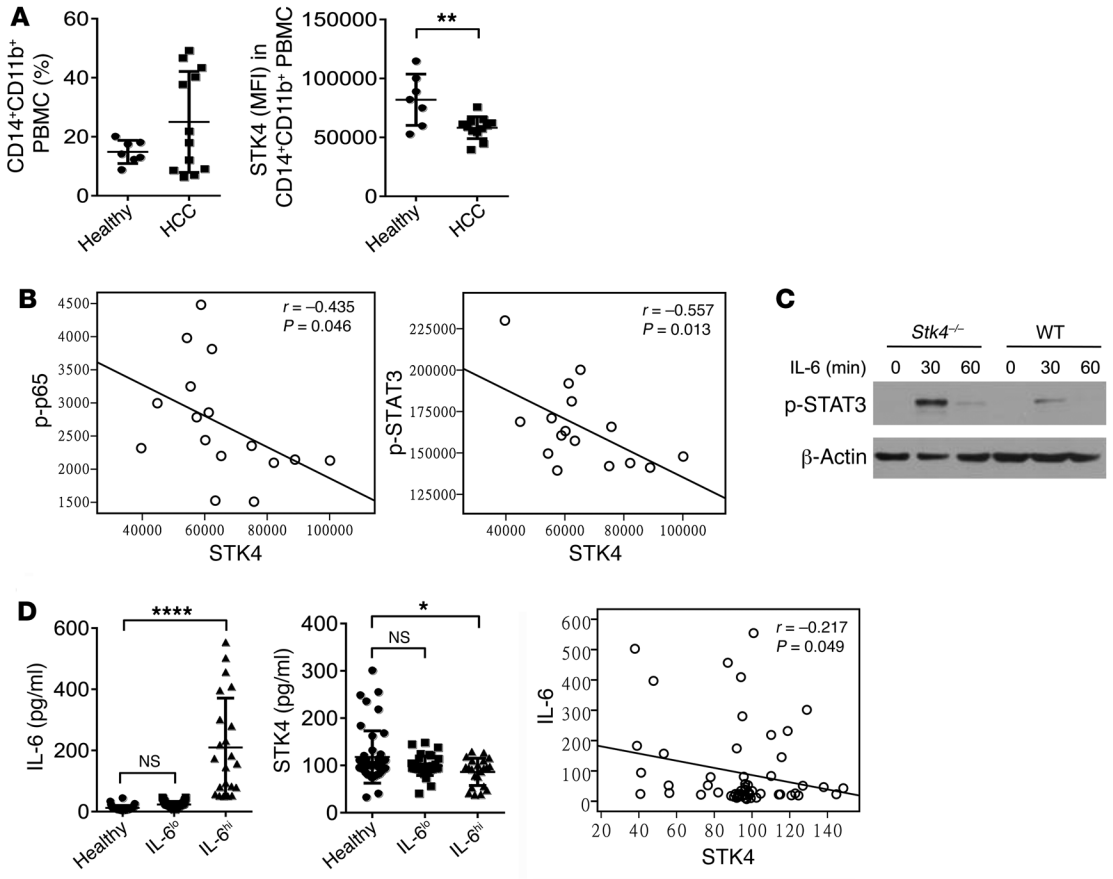

Figure 10. STK4 expression is inversely correlated with the levels of p-p65 and p-STAT3 in macrophages from human HCC samples. (**A** and **B**) PBMCs from healthy (n = 7) and HCC patients (n = 12) were stained with anti-CD11b, anti-CD14, anti-STK4, anti-phospho65, and anti-phosphoSTAT3 for FACS analysis (2-tailed, unpaired Student's t test), and their correlation (n = 16) was determined by Pearson's test. (**C**) p-STAT3 levels were examined by immunoblotting in WT and *Stk4*$^{-/-}$ BMMs after IL-6 (100 ng/ml) treatment. (**D**) Plasma IL-6 and STK4 concentrations were evaluated from healthy (n = 40) and HCC patients (n = 59) to analyze their correlation using Pearson's test. One-way ANOVA with Holm-Sidak's multiple comparisons test was used. Data represent mean ± SD. *P < 0.05, **P < 0.01, and ****P < 0.0001.

opment of HCC (13), we observed that *Stk4* deficiency showed no significant effect on apoptosis in resting, LPS-treated, or poly(I:C)-treated macrophages (Supplemental Figure 7). Next, we cross-bred mice bearing loxP sites flanking exons 4–5 of the *Stk4* gene (i.e., *Stk4*$^{fl/fl}$) with lysozyme (*Lysm-Cre*) mice to specifically knock out STK4 expression in macrophages (termed *Stk4*$^{\Delta M/\Delta M}$ mice). *Stk4*$^{\Delta M/\Delta M}$ mice and their WT *Stk4*$^{+/+}$ littermates were treated with DEN and hepatotoxin carbon tetrachloride (CCl_4) in combination with low doses of LPS to generate a chronic inflammation–associated liver cancer model, as previously reported (ref. 3 and Figure 7A). Compared with the WT controls, IL-6 concentrations in the serum were enhanced in *Stk4*$^{\Delta M/\Delta M}$ mice 48 hours after DEN treatment (Figure 7B, left panel). *Stk4*$^{\Delta M/\Delta M}$ mice exhibited further-enhanced serum IL-6 levels after injection of DEN, plus 2 subsequent injections of CCl_4 with daily LPS treatment for 2 weeks (Figure 7B, right panels). Furthermore, mRNA levels of *Il6*, *Il1b*, and *Ccl2* were increased and *Ifnb* mRNA levels were reduced in the livers of *Stk4*$^{\Delta M/\Delta M}$ mice (Figure 7B, right panels). In line with this, we observed excessive accumulation of immune cells by HE staining and more apoptotic cells by TUNEL staining in the livers of *Stk4*$^{\Delta M/\Delta M}$ mice (Figure 7C). The liver injury determined by serum alanine aminotransferase (ALT) and aspartate aminotransferase (AST) levels was also exacerbated in these *Stk4*$^{\Delta M/\Delta M}$ mice (Figure 7D). Taken together, our data show that *Stk4*$^{\Delta M/\Delta M}$ mice displayed heightened inflammation and liver injury at the early stage (at 6 weeks) after treatment with DEN, CCl_4, and LPS.

Dying hepatocytes release various mediators to support myofibroblast proliferation and extracellular matrix production, which lead to the induction of liver fibrosis. During chronic liver damage–induced inflammation, fibrosis acts as a precursor of cirrhosis, and the liver cytoarchitecture is eventually disrupted by excessive extracellular matrix deposition (42). We next detected liver fibrosis at the late stage (7 months) after DEN, CCl_4, and LPS treatment by Sirius Red staining, which showed heavier liver fibrosis in *Stk4*$^{\Delta M/\Delta M}$ mice than in WT mice (Figure 7E). Moreover, *Stk4*$^{\Delta M/\Delta M}$ mice increased numbers and size of tumors compared with WT controls (Figure 7F).

Recently, studies have suggested that when liver physiology is disrupted, gut microflora (especially gram-negative bacteria) propagate inflammation and thereby exacerbate liver fibrosis or liver carcinoma (43). Moreover, clinical studies have demonstrated that bacterial infections of the liver are frequently detected and involved in the process of inflammation-associated human cirrhosis or HCC (44). To mimic pathogen infection–induced

HCC, we established a mouse model using DEN and CCl_4 treatment, plus monthly *E. coli* infection to induce chronic inflammation and liver cancer (Figure 8A). Similar to the LPS-treated HCC model, serum IL-6 levels were increased at the early stage after DEN and CCl_4 treatment, plus *E. coli* infection (11 weeks) (Figure 8B). We also detected more liver injury in *Stk4*$^{\Delta M/\Delta M}$ mice, as determined by serum ALT and AST levels after DEN treatment, plus 10 injections of CCl_4 and 2 rounds of *E. coli* infection (Figure 8C). By 36 weeks, we detected increased levels of fibrillar collagen deposition around portal veins by Sirius Red staining in the livers of *Stk4*$^{\Delta M/\Delta M}$ mice (Figure 8D). Moreover, *Stk4*$^{\Delta M/\Delta M}$ mice displayed more liver tumors with the disrupted liver cytoarchitecture shown by HE staining (Figure 8E), and enhanced expression of the oncogene *H19*, as well as the cell proliferation gene *Ki67* (Figure 8F). Collectively, we have established 2 different mouse models to demonstrate the protective role of STK4 in macrophages during chronic inflammation–induced HCC.

Because macrophage plasticity (i.e., polarization into M1 versus M2 macrophages) has key roles in tumorigenesis, we assessed whether STK4 also regulates M2-associated gene expression — including *Arg1*, *Ym1, Fizz1*, and *Il10* expression — during the process of HCC. The mRNA levels of *Arg1*, *Ym1*, *Fizz1*, and *Il10* were comparable between WT and *Stk4*$^{\Delta M/\Delta M}$ mice at the early stage (5 weeks) or late stage (7 and 9 months) after treatment with DEN, CCl4, and LPS (Supplemental Figure 8, A–C). Moreover, we did not observe significant changes in mRNA levels *of Arg1*, *Ym1*, and *Fizz1* between WT and *Stk4*$^{-/-}$ macrophages that had been stimulated with IL-4 and IL-13 in vitro (Supplemental Figure 8D). We suggest that during chronic inflammation–induced HCC, STK4 in macrophages might mainly regulate the production of proinflammatory cytokines.

The inverse correlation of STK4 expression with the levels of IRAK1, IL-6, phospho-p65 and phospho-STAT3 in macrophages from human HCC samples. The next crucial question was to ask whether STK4 expression in macrophages is relevant to human HCC. Samples from HBV-infected HCC patients were collected and compared with those from controls. First, compared with paracarcinoma tissue, more $CD68^+$ macrophages accumulated in human liver tumors, as determined by IHC staining (Figure 9A). In contrast, much less expression of STK4 was detected in human liver tumors than in paracarcinoma tissue, and this was inversely correlated with IRAK1 staining (Figure 9A). Because we showed in Figure 5 that STK4 phosphorylates IRAK1 and promotes IRAK1 degradation, thereby differentially regulating the TLR3/4 pathways, the next key issue was whether STK4 expression correlates with IRAK1 levels in macrophages in human HCC. To investigate this, we stained the adjacent liver tissue sections with anti-CD68, anti-STK4, and anti-IRAK1. Compared with the adjacent healthy liver tissue, STK4 expression was decreased in tumor-infiltrating macrophages identified by $CD68^+$ staining; in contrast, IRAK1 was expressed at relatively higher levels in these macrophages (Figure 9B). To further confirm this, we labeled intrahepatic macrophages from human HCC samples using anti-CD11b staining and then analyzed the expression levels of STK4 and IRAK1 by FACS analysis. We revealed that STK4 expression inversely correlated with IRAK1 levels in these tumor-infiltrating macrophages (Figure 9C).

Considering that IRAK1 plays key roles for proinflammatory cytokine production in macrophages, as well as for cell proliferation in liver tumor cells, we examined the possibility to target IRAK1 for antiinflammation and antitumor treatment. WT and *Stk4* KO mice were i.p. injected with the IRAK1/4 inhibitor, starting 1 week before the first CCl_4 injection. In response to the IRAK1/4 inhibitor, serum IL-6 levels were significantly reduced in *Stk4* KO mice to similar levels as those in WT mice at the early stage after DEN, CCl_4, and LPS treatment (6 weeks after DEN treatment, Figure 9D, left panel). Liver tumor formation was detected by micro-CT imaging 18 weeks after DEN treatment (Supplemental Figure 9). *Stk4* KO mice displayed more tumors than WT control mice; however, after treatment with the IRAK1/4 inhibitor, *Stk4* KO mice reduced the number of liver tumors to similar degree as those in WT mice (Figure 9D, right panel).

Interestingly, compared with healthy donors, we found higher percentages of $CD14^+CD11b^+$ monocytes/macrophages in the blood of HCC patients, and these cells had significantly downregulated STK4 expression (Figure 10A and Supplemental Figure 10A). More importantly, FACS analysis revealed that the phosphorylation levels of p65, as well as STAT3, inversely correlated with STK4 expression in $CD14^+CD11b^+$ monocytes/macrophages from the blood of HCC patients (Figure 10B). To further confirm this, we also analyzed $CD11b^+$ macrophages/KCs from the liver tumors of HCC patients, which indeed showed that STK4 expression inversely correlated with the phosphorylation levels of p65 and STAT3 (Supplemental Figure 10B). Previous studies have shown that STAT3 is constitutively activated both in tumor cells and in immune cells in the human tumor microenvironment, resulting in not only the upregulation of genes crucial for survival, proliferation, angiogenesis, and metastasis, but also induction of expression of immune suppressive factors. To examine the connection between STK4 and STAT3, WT and *Stk4*$^{-/-}$ macrophages were treated with IL-6 ex vivo. In line with the inverse association between STK4 expression and phospho-Stat3 (p-STAT3) levels, we observed that p-STAT3 levels were increased in *Stk4*$^{-/-}$ macrophages (Figure 10C). We also sequenced p53 and STAT3 in human HCC samples and identified p53 mutations in most of the samples, while there was no correlation between p53 or STAT3 mutations and the expression levels of *Stk4* or IL-6 (Supplemental Table 2). We next investigated whether there is any correlation of *p53* or *STAT3* and *STK4* at mRNA levels in human HCC samples. Data of 369 HCC samples provided by the TCGA program were analyzed, and no significant correlation was identified (Supplemental Figure 10C).

Because plasma STK4 concentrations can be detected by a method such as ELISA, we next asked whether plasma STK4 could be used as a new biomarker to identify a specific population of human HCC patients. We collected blood samples from healthy patients (n = 45) and HCC patients (n = 59). Based on the plasma IL-6 levels, we divided the HCC patients into 2 groups with different degrees of inflammation (i.e., serum IL-6^{lo} versus serum IL-6^{hi}) (Figure 10D, left panel). Interestingly, we observed a significant reduction in the plasma STK4 concentration only in IL-6^{hi} HCC patients compared with healthy controls (Figure 10D, middle panel). Additionally, an inverse correlation was detected between the plasma IL-6 levels and plasma STK4 concentrations in HCC patients (Figure 10D, right panel). Next, we compared the levels of genome transcripts from IL-6^{lo}STK4^{hi} versus IL-6^{hi}STK4^{lo} human liver tumors. In agreement with the role of STK4, genes

related to cell cycle arrest and chromatin condensation were elevated in IL-6^{lo}STK4^{hi} samples, while genes related to inflammation and proliferation were highly expressed in IL-6^{hi}STK4^{lo} samples (Supplemental Figure 10D). We therefore suggest that plasma STK4 might be a new biomarker for a group of HCC patients who display a relatively high degree of inflammation.

Furthermore, we noted that treatment with exogenous IL-1β or LPS, or infection with bacterial SL1344 reduced the mRNA levels of *Stk4* in murine primary hepatocytes (Supplemental Figure 10E, left panel). Importantly, the human cell line HepG2 also had decreased *Stk4* expression after stimulation with exogenous IL-6, IL-1β, or TNF-α (Supplemental Figure 10F, left panel). In addition, we measured the mRNA levels of *Ccl2*, *Il1b*, and *Il6* in murine primary hepatocytes (Supplemental Figure 10E, right panels) or human HepG2 cells (Supplemental Figure 10F, right panels). Interestingly, after stimulation with the proinflammatory cytokines or LPS, or infection with SL1344, murine or human hepatocytes enhanced the production of *Ccl2*, *Il1b* and *Il6*. This suggests that *Stk4* is a critical antiinflammatory gene and its expression is downregulated to induce inflammatory responses in macrophages after infection; inflammation then triggers downregulation of STK4 expression in hepatocytes, which results in further enhancement of inflammation by hepatocytes or liver tumor cells (see the model in Supplemental Figure 10G).

Our study collected data from murine models and clinical HCC samples and demonstrated that STK4 in macrophages plays a protective role during chronic inflammation–induced HCC via IRAK1 in a cell-intrinsic manner. We have provided evidence showing that, in addition to being a tumor suppressor, STK4 acts as an antiinflammatory regulator in macrophages and thereby blocks chronic inflammation–associated HCC.

Discussion

The association between chronic inflammation and human cancers has been extensively studied. Recent studies have identified several key tumor suppressors that can play a dual role in inducing inflammation and cancer (2). STK4 is a key TSG in HCC and is generally expressed in immune cells. However, its regulatory role in TLR pathway–mediated inflammatory responses and in inflammation-associated HCC is not fully understood. In addition, to our knowledge, only a few key regulators (such as SHP-1) have been identified to inhibit NF-κB–mediated inflammation but enhance IRF-3–mediated IFN production via different TLR pathways (32).

This study revealed that STK4 has an inhibitory function in the TLR4/9-mediated production of proinflammatory cytokines, including IL-6, IL-1β, and TNF-α. In contrast, STK4 heightens TLR3/4-induced type-I IFN production. This might be due to the fact that STK4 can bind to and phosphorylate IRAK1. Previous reports have suggested that IRAK1 is an important component of TLR pathways and that it differentially regulates the activation of NF-κB and IRF3 (33, 34). Moreover, the phosphorylation of IRAK1 at its ser/thr sites activates IRAK1, leading to its degradation by a proteasome-dependent process (35). Our study applied several strategies — including the use of an IRAK1 inhibitor, specific siRNA, and a luciferase reporter system — and demonstrated that IRAK1 is indispensable for the regulatory role of STK4 in the TLR3/4/9 pathways. We therefore propose that the STK4-IRAK1 module represents a unique signaling complex that differentially regulates the TLR3/4/9-mediated production of proinflammatory cytokines and type-I IFNs.

Persistent infection and infiltration of immune cells into infection sites can lead to chronic inflammation, which is closely linked to HCC development. Recent efforts have revealed several essential effectors that act as both tumor suppressors and anti-inflammation regulators, thereby linking immune cell–mediated inflammation and tumorigenic progress in hepatocytes. For example, the ubiquitin-editing enzyme A20 (also termed TNFAIP3) is a tumor suppressor that blocks tumor cell–intrinsic NF-κB signals (45). A20 has recently been identified in myeloid cells and targets TRAF6, MALT1, or NEMO for degradation, thereby restraining the TLR-induced inflammatory response (46). Similar to the dual role of A20, the deubiquitination enzyme cylindromatosis (CYLD) not only acts as a tumor suppressor, but also suppresses the TLR/NF-κB–dependent inflammatory response in macrophages (40, 47, 48). Therefore, A20 and CYLD have been proposed as biomarkers that link protumorigenic inflammation to tumorigenesis. This study identified that, in addition to the above enzymes, the kinase STK4 also functions in both immune cells and hepatocytes to suppress chronic inflammation–associated HCC. Additionally, STK4 enhances TLR3/4-mediated IFN-β production. It has been demonstrated that IFN-β facilitates the clearance of invading pathogens (49, 50). In addition, IFN-β treatment reduces the risk of HCV-associated HCC (51). Considering that there are currently no available murine models that precisely mimic HBV infection–induced HCC in humans, we were unable to examine the relevant role of STK4-mediated IFN-β production in alleviating the development of HCC.

To investigate whether the kinase STK4 is a potential biomarker, we induced inflammation-associated HCC using DEN and CCl_4 in combination with low-dose LPS stimulation, as the previous study reported (3). Moreover, we generated a new chronic inflammation–induced HCC murine model using monthly *E. coli* infection (instead of LPS treatment). These 2 models incorporate chronic inflammation, as well as liver injury and fibrogenesis, thus mimicking the development of inflammation-associated HCC in human patients. With these animal models, we showed that macrophage-specific deletion of *Stk4* enhanced the production of IL-6, IL-1β, and CCL2 and decreased the production of IFN-β in the liver. Previous studies have reported that long-lasting chronic inflammation mediated by immune cells may lead to the induction of oncogenic mutations. Furthermore, the local inflammatory environment promotes tumor cell secretion of chemokines such as CCL2, thereby recruiting more immune cells and elevating IL-1β and IL-6 levels, which feed back to promote hepatoma cell proliferation (52). In agreement with this scenario, our data showed that proinflammatory cytokines or bacterial infections reduced STK4 expression and enhanced proinflammatory cytokine and CCL2 production in hepatocytes. In addition, we observed that tumor-infiltrating T cells reduced STK4 expression (Supplemental Figure 1F). Previous studies have demonstrated that STK4 is critical for naive T cell survival and immune surveillance against infections, while human immunodeficiency phenotype is associated with *Stk4* deficiency or mutation and primarily characterized by a progressive loss of naive T cells (15, 53, 54). This suggests that

STK4 reduction regulates the crosstalk between macrophages and liver tumor cells to exacerbate inflammation, which might also result in reduced T cell–mediated immune surveillance, eventually rendering *Stk4*$^{\Delta M/\Delta M}$ mice more susceptible to liver damage and subsequent tumor formation.

Because the current chemotherapy for HCC is not effective, identification of the molecular markers correlating with early diagnosis of HCC is essential for effective prevention of progression. Our study has provided the first evidence that the IL-6^{hi} population of HCC patients displays reduced plasma STK4 concentrations. This suggests that plasma STK4 might be a new biomarker of inflammation-associated human HCC, showing improved cost effectiveness and high-throughput screening of high-risk populations (e.g., HBV- or HCV-infected subjects with defective liver function) for early detection of inflammation-associated HCC. We further demonstrated that reduced STK4 expression is inversely correlated with the levels of the downstream targets IRAK1, phospho-p65 (p-p65), and p-STAT3 in macrophages from human HCC samples. Previous reports suggest that activation of STAT3 or NF-κB is enhanced in human HCC (55–57). Considering that IRAK1 and NF-κB play key roles in proinflammatory cytokine production and in liver tumor cell proliferation, we and others showed that inhibitors of IRAK1 and NF-κB could be used against leukemia and HCC (Figure 9D and refs. 58, 59). Notably, serum STK4 levels have been suggested for the diagnosis of colorectal cancer, which is also a chronic inflammation–associated cancer (60). Future work should address in detail whether STK4 is a biomarker in other types of inflammation-associated tumors, such as gastric carcinoma, and whether and how STK4 expression is correlated with the activation status of NF-κB and STAT3 in tumor cells. These findings might propose STK4 as a promising strategy for interrupting the proinflammatory microenvironment and blocking HCC.

Methods

Further information can be found in Supplemental Methods.

Mice. *Stk4*$^{fl/fl}$ mice bearing loxP sites flanking exons 4-5 of the *Stk4* gene were cross-bred with *Lysm-Cre* mice to specifically knock out *Stk4* expression in the myeloid cell lineage, including macrophages (termed *Stk4*$^{\Delta M/\Delta M}$ mice). *Stk4*$^{fl/fl}$, *Stk4*$^{-/-}$, and *Stk3*$^{-/-}$ mice on the 129Sv background were obtained from the Tao lab at Fudan University, Shanghai, China. *Stk4*$^{\Delta M/\Delta M}$ mice were backcrossed to a 129Sv background 3 times. *Stk4*$^{\Delta M/\Delta M}$, *Stk4*$^{-/-}$, and *Stk3*$^{-/-}$ mice or their littermates were bred and maintained under Specific Pathogen Free (SPF) conditions in the institutional animal facility of the Shanghai Institute of Biochemistry and Cell Biology. Age- and sex-matched littermates were used as control mice. All in vivo and in vitro experiments were performed on 8- to 12-week-old mice.

Induction of chronic inflammation–associated HCC model. The WT male littermates *Stk4*$^{+/+}$ and *Stk4*$^{\Delta M/\Delta M}$ mice (8 weeks) were i.p. injected with DEN (100 mg/kg). Four weeks later, mice were weekly i.p. injected with CCl_4 (0.5 ml/kg, dissolved in olive oil) for 12 weeks. Low doses of LPS were applied to induce inflammation-associated HCC as previously described (3). One week before the first CCl_4 injection, DEN-treated mice were s.c. injected with LPS (300 μg/kg/d) for 12 weeks. Alternatively, DEN-treated mice were monthly i.v. injected with *E. coli* (5×10^3 CFU) 4 times. Mice were sacrificed 28–36 weeks after the initial DEN injection to evaluate the development of HCC. For in vivo treatment of the IRAK1/4 inhibitor, WT or *Stk4* KO mice were i.p. injected with the IRAK1/4 inhibitor (3 mg/kg, twice a week, starting 1 week before the first CCl_4 injection) for 9 weeks. Serum IL-6 was assessed 6 weeks after DEN treatment by ELISA, while liver tumor formation was detected by micro-CT imaging 18 weeks after DEN treatment.

Micro-CT imaging. The micro-CT contrast agent Fenestra LC nano-emulsions are manufactured by sheer-induced rupturing of lipids with 10% iodinated triglycerides (MediLumine). The particle size of lipid spheres are under 150 nm, which could pass through fenestrae in hepatic portal vessels and access hepatocytes. The iodine concentration in Fenestra LC is 50 mg/ml, and mice were i.v. injected in a dose of 7.5 ml/kg and imaged at 4 hours after injection. Mice were anesthetized with isoflurance inhalation and scanned with the micro-CT from PerkinElmer. The scanning protocol was programmed to acquire images while continuously rotating mice by 360° within 14 minutes, and the images were analyzed using the software provided by PerkinElmer. In the 2-D images, tumors were shown with lower density. Three-D virtual-reality and rendering software was used to create 3-D transparent simulations, showing tumors in green and livers in pink.

Induction of endotoxin shock. For endotoxin shock induction, WT and *Stk4*$^{-/-}$ mice were i.p. injected with LPS (3 mg/per mouse). Three days later, serum was collected to measure concentrations of IL-6 and TNF-α by ELISA (eBioscience), and lung tissue damage was assessed by HE staining.

Histological analysis. Paraffin-embedded samples were prepared from lung or liver of the experimental mice or HCC patients. HE or Sirius Red dissolved in saturated picric acid (0.1%) was used to stain liver sections. TUNEL assays were performed using the ApoAlert DNA Fragmentation Assay Kit (Clontech). Liver injury was assessed via measuring ALT and AST activity in serum. Blood and liver tumor samples from HCC patients were obtained from Huadong Hospital, Wuhan Tumor Hospital, and Zhongshan Hospital, Shanghai, China. Blood from healthy donors was from Huashan Hospital, Shanghai, China.

Cell culture. PEMs were harvested from mice with i.p. injection of 3% Brewer thioglycollate medium. BM cells were cultured with L929-conditioned completed DMEM medium for a week to generate BMMs. Infiltrated immune cells in liver tissue were isolated by isodensity centrifugation with Percoll (GE Healthcare; catalog 17-0891-01). PBMC were prepared from human blood using lymphocyte separation medium (MP Biomedicals). Primary murine PEMs, BMMs, MEF cells, fresh isolated hepatocytes, HEK293T, and RAW264.7 cell lines were cultured in complete DMEM supplemented with 10% (v/v) FBS and 1% penicillin/streptomycin (100 U/ml) at 37°C with 5% CO_2.

Statistics. Statistical data analysis was performed with Graphpad Prism 6.0 software. Data represent mean ± SD. Statistical significance was determined with 2-tailed unpaired Student's *t* test between 2 groups. One-way or 2-way ANOVA with Holm-Sidak correction or with Newman-Keuls correction were used for multiple comparisons. Correlations were done using Pearson's or Spearman's tests. $P < 0.05$ was considered statistically significant ($^*P < 0.05$, $^{**}P < 0.01$, $^{***}P < 0.001$, and $^{****}P < 0.0001$).

Study approval. All animal procedures were conducted in strict accordance with the institutional guidelines and were approved by the Institutional Animal Care and Use Committee of Shanghai Institute of

Biochemistry and Cell Biology (IBCB0057). For human samples, the study was approved by the Ethical Committee for Clinical Research of the participating hospitals.

Acknowledgments

This work was supported by grants from the Ministry of Science and Technology of China (2012CB910800); National Natural Science Foundation of China (31422018, 81571617, 81571552, 31300723, and 81590764); WIV "One-Three-Five" Strategic Programs for B. Wei; Shanghai Pujiang program (11PJ1410700) for H. Wang; and funding from Cancer Research Center, Xuhui Central Hospital (CCR2012005). H. Wang is supported by the Hundred Talents Program of the Chinese Academy of Sciences.

Address correspondence to: Bin Wei, Wuhan Institute of Virology, Chinese Academy of Sciences, Xiao Hong Shan Road 44, Wuhan, 430071, China. Phone: 0086.27.87197366; E-mail: weibin@wh.iov.cn. Or to: Hongyan Wang, Institute of Biochemistry and Cell Biology, Shanghai Institutes for Biological Sciences, Chinese Academy of Sciences, 320 Yue-yang Road, Shanghai, 200031, China. Phone: 0086.21.54921086; E-mail: hongyanwang@sibcb.ac.cn.

1. Hussain SP, Harris CC. Inflammation and cancer: an ancient link with novel potentials. *Int J Cancer*. 2007;121(11):2373–2380.
2. Yang L, Karin M. Roles of tumor suppressors in regulating tumor-associated inflammation. *Cell Death Differ*. 2014;21(11):1677–1686.
3. Dapito DH, et al. Promotion of hepatocellular carcinoma by the intestinal microbiota and TLR4. *Cancer Cell*. 2012;21(4):504–516.
4. Aksoy E, et al. The p110delta isoform of the kinase PI(3)K controls the subcellular compartmentalization of TLR4 signaling and protects from endotoxic shock. *Nat Immunol*. 2012;13(11):1045–1054.
5. Liew FY, Xu D, Brint EK, O'Neill LA. Negative regulation of toll-like receptor-mediated immune responses. *Nat Rev Immunol*. 2005;5(6):446–458.
6. Zhang Y, et al. Activation of vascular endothelial growth factor receptor-3 in macrophages restrains TLR4-NF-κB signaling and protects against endotoxin shock. *Immunity*. 2014;40(4):501–514.
7. Bard-Chapeau EA, et al. Ptpn11/Shp2 acts as a tumor suppressor in hepatocellular carcinogenesis. *Cancer Cell*. 2011;19(5):629–639.
8. Gautheron J, Luedde T. A novel player in inflammation and cancer: the deubiquitinase CYLD controls HCC development. *J Hepatol*. 2012;57(5):937–939.
9. Takahashi H, Ogata H, Nishigaki R, Broide DH, Karin M. Tobacco smoke promotes lung tumorigenesis by triggering IKKβ- and JNK1-dependent inflammation. *Cancer Cell*. 2010;17(1):89–97.
10. Li L, et al. A unique role for p53 in the regulation of M2 macrophage polarization. *Cell Death Differ*. 2015;22(7):1081–1093.
11. Cooks T, et al. Mutant p53 prolongs NF-κB activation and promotes chronic inflammation and inflammation-associated colorectal cancer. *Cancer Cell*. 2013;23(5):634–646.
12. Wu H, et al. Integration of Hippo signaling and the unfolded protein response to restrain liver overgrowth and tumorigenesis. *Nat Commun*. 2015;6:6239.
13. Zhou D, et al. Mst1 and Mst2 maintain hepatocyte quiescence and suppress hepatocellular carcinoma development through inactivation of the Yap1 oncogene. *Cancer Cell*. 2009;16(5):425–438.
14. Kim TS, Lee DH, Kim SK, Shin SY, Seo EJ, Lim DS. Mammalian sterile 20-like kinase 1 suppresses lymphoma development by promoting faithful chromosome segregation. *Cancer Res*. 2012;72(20):5386–5395.
15. Nehme NT, et al. MST1 mutations in autosomal recessive primary immunodeficiency characterized by defective naive T-cell survival. *Blood*. 2012;119(15):3458–3468.
16. Zhou D, et al. The Nore1B/Mst1 complex restrains antigen receptor-induced proliferation of naive T cells. *Proc Natl Acad Sci U S A*. 2008;105(51):20321–20326.
17. Katagiri K, Imamura M, Kinashi T. Spatiotemporal regulation of the kinase Mst1 by binding protein RAPL is critical for lymphocyte polarity and adhesion. *Nat Immunol*. 2006;7(9):919–928.
18. Zhang YB, Wang HY. Integrin signaling and function in immune cells. *Immunology*. 2012;135(4):268–275.
19. Wang HY, Lim D, Rudd CE. Immunopathologies linked to integrin signaling. *Semin Immunopathol*. 2010;32(2):173–182.
20. Raab M, et al. T cell receptor "inside-out" pathway via signaling module SKAP1-RapL regulates T cell motility and interactions in lymph nodes. *Immunity*. 2010;32(4):541–556.
21. Wang H, Rudd CE. SKAP-55, SKAP-55-related and ADAP adaptors modulate integrin-mediated immune-cell adhesion. *Trends Cell Biol*. 2008;18(10):486–493.
22. Li C, et al. ADAP and SKAP55 deficiency suppresses PD-1 expression in $CD8^+$ cytotoxic T lymphocytes for enhanced anti-tumor immunotherapy. *EMBO Mol Med*. 2015;7(6):754–769.
23. Schneider H, et al. Adaptor SKAP-55 binds p21 activating exchange factor RasGRP1 and negatively regulates the p21-ERK pathway in T-cells. *PLoS One*. 2008;3(3):e1718.
24. MacIver NJ, et al. The liver kinase B1 is a central regulator of T cell development, activation, and metabolism. *J Immunol*. 2011;187(8):4187–4198.
25. Zhang YG, et al. Axin1 prevents Salmonella invasiveness and inflammatory response in intestinal epithelial cells. *PLoS One*. 2012;7(4):e34942.
26. Bleriot C, Dupuis T, Jouvion G, Eberl G, Disson O, Lecuit M. Liver-resident macrophage necroptosis orchestrates type 1 microbicidal inflammation and type-2-mediated tissue repair during bacterial infection. *Immunity*. 2015;42(1):145–158.
27. Mencin A, Kluwe J, Schwabe RF. Toll-like receptors as targets in chronic liver diseases. *Gut*. 2009;58(5):704–720.
28. Liaunardy-Jopeace A, Gay NJ. Molecular and cellular regulation of toll-like receptor-4 activity induced by lipopolysaccharide ligands. *Front Immunol*. 2014;5:473.
29. McGettrick AF, O'Neill LA. Localisation and trafficking of Toll-like receptors: an important mode of regulation. *Curr Opin Immunol*. 2010;22(1):20–27.
30. Cinar B, et al. The pro-apoptotic kinase Mst1 and its caspase cleavage products are direct inhibitors of Akt1. *EMBO J*. 2007;26(21):4523–4534.
31. Du X, et al. Mst1/Mst2 regulate development and function of regulatory T cells through modulation of Foxo1/Foxo3 stability in autoimmune disease. *J Immunol*. 2014;192(4):1525–1535.
32. An H, et al. Phosphatase SHP-1 promotes TLR- and RIG-I-activated production of type I interferon by inhibiting the kinase IRAK1. *Nat Immunol*. 2008;9(5):542–550.
33. Bruni D, Sebastia J, Dunne S, Schroder M, Butler MP. A novel IRAK1-IKKε signaling axis limits the activation of TAK1-IKKβ downstream of TLR3. *J Immunol*. 2013;190(6):2844–2856.
34. Murakami Y, Mizoguchi F, Saito T, Miyasaka N, Kohsaka H. p16(INK4a) exerts an anti-inflammatory effect through accelerated IRAK1 degradation in macrophages. *J Immunol*. 2012;189(10):5066–5072.
35. Yamin TT, Miller DK. The interleukin-1 receptor-associated kinase is degraded by proteasomes following its phosphorylation. *J Biol Chem*. 1997;272(34):21540–21547.
36. Gottipati S, Rao NL, Fung-Leung WP. IRAK1: A critical signaling mediator of innate immunity. *Cell Signal*. 2008;20(2):269–276.
37. Johnson C, Han Y, Hughart N, McCarra J, Alpini G, Meng F. Interleukin-6 and its receptor, key players in hepatobiliary inflamzmation and cancer. *Transl Gastrointest Cancer*. 2012;1(1):58–70.
38. Mano Y, et al. Tumor-associated macrophage promotes tumor progression via STAT3 signaling in hepatocellular carcinoma. *Pathobiology*. 2013;80(3):146–154.
39. Naugler WE, et al. Gender disparity in liver cancer due to sex differences in MyD88-dependent IL-6 production. *Science*. 2007;317(5834):121–124.
40. Nikolaou K, Tsagaratou A, Eftychi C, Kollias G, Mosialos G, Talianidis I. Inactivation of the deubiquitinase CYLD in hepatocytes causes apoptosis, inflammation, fibrosis, and cancer. *Cancer Cell*. 2012;21(6):738–750.
41. Lin FC, Young HA. Interferons: Success in anti-viral immunotherapy. *Cytokine Growth Factor Rev*. 2014;25(4):369–376.
42. Bataller R, Brenner DA. Liver fibrosis. *J Clin Invest*. 2005;115(2):209–218.
43. Son G, Kremer M, Hines IN. Contribution of gut bacteria to liver pathobiology. *Gastroenterol Res*

Pract. 2010;2010:453563.
44. Agha-Amiri K, Klauck S, Malfertheiner P. Bacterial infection is frequent in human hepatocellular carcinoma (HCC), but not in liver cirrhosis. *Gastroenterology*. 2000;118(4 part 1):A321.
45. Schmitz R, et al. TNFAIP3 (A20) is a tumor suppressor gene in Hodgkin lymphoma and primary mediastinal B cell lymphoma. *J Exp Med*. 2009;206(5):981–989.
46. Ma A, Malynn BA. A20: linking a complex regulator of ubiquitylation to immunity and human disease. *Nat Rev Immunol*. 2012;12(11):774–785.
47. Bignell GR, et al. Identification of the familial cylindromatosis tumour-suppressor gene. *Nat Genet*. 2000;25(2):160–165.
48. Yoshida H, Jono H, Kai H, Li JD. The tumor suppressor cylindromatosis (CYLD) acts as a negative regulator for toll-like receptor 2 signaling via negative cross-talk with TRAF6 AND TRAF7. *J Biol Chem*. 2005;280(49):41111–41121.
49. Stifter SA, Feng CG. Interfering with immunity: detrimental role of type I IFNs during infection. *J Immunol*. 2015;194(6):2455–2465.
50. Perry AK, Chen G, Zheng D, Tang H, Cheng G. The host type I interferon response to viral and bacterial infections. *Cell Res*. 2005;15(6):407–422.
51. Takeyasu M, et al. Long-term interferon monotherapy reduces the risk of HCV-associated hepatocellular carcinoma. *J Med Virol*. 2012;84(8):1199–1207.
52. Sakurai T, et al. Hepatocyte necrosis induced by oxidative stress and IL-1α release mediate carcinogen-induced compensatory proliferation and liver tumorigenesis. *Cancer Cell*. 2008;14(2):156–165.
53. Abdollahpour H, et al. The phenotype of human STK4 deficiency. *Blood*. 2012;119(15):3450–3457.
54. Crequer A, et al. Inherited MST1 deficiency underlies susceptibility to EV-HPV infections. *PLoS One*. 2012;7(8):e44010.
55. Zuo M, Li C, Lin J, Javle M. LLL12, a novel small inhibitor targeting STAT3 for hepatocellular carcinoma therapy. *Oncotarget*. 2015; 6(13):10940–10949.
56. He G, Karin M. NF-κB and STAT3 — key players in liver inflammation and cancer. *Cell Res*. 2011;21(1):159–168.
57. Arsura M, Cavin LG. Nuclear factor-κB and liver carcinogenesis. *Cancer Lett*. 2005;229(2):157–169.
58. Li Z, et al. Inhibition of IRAK1/4 sensitizes T cell acute lymphoblastic leukemia to chemotherapies. *J Clin Invest*. 2015;125(3):1081–1097.
59. Saeki I, et al. Bortezomib induces tumor-specific cell death and growth inhibition in hepatocellular carcinoma and improves liver fibrosis. *J Gastroenterol*. 2013;48(6):738–750.
60. Zhai XH, Yu JK, Yang FQ, Zheng S. Identification of a new protein biomarker for colorectal cancer diagnosis. *Mol Med Rep*. 2012;6(2):444–448.